1 **Tropical tropospheric ozone distribution and trends from in situ and satellite**
2 **data**

3

4

5 **Audrey Gaudel[1,2*], Ilann Bourgeois[1,2,#], Meng Li[1,2], Kai-Lan Chang[1,2], Jerald Ziemke[3,4],**
6 **Bastien Sauvage[5], Ryan M. Stauffer[3], Anne M. Thompson[3,6], Debra E. Kollonige[3,7], Nadia**
7 **Smith[8], Daan Hubert[9], Arno Keppens[9], Juan Cuesta[10], Klaus-Peter Heue[11], Pepijn**
8 **Veefkind[12,13], Kenneth Aikin[1,2], Jeff Peischl[1,2], Chelsea R. Thompson[2], Thomas B. Ryerson[2],**
9 **Gregory J. Frost[2], Brian C. McDonald[2], Owen R. Cooper[1,2]**

10

11 **[1]CIRES, University of Colorado, Boulder, USA**

12 **[2]NOAA Chemical Sciences Laboratory, Boulder, USA**

13 **[3]NASA Goddard Space Flight Center, Greenbelt, Maryland, USA**

14 **[4]Morgan State University, Baltimore, Maryland, USA**

15 **[5]Laboratoire d'Aérologie, Université de Toulouse, CNRS, Université Toulouse III Paul**
16 **Sabatier, France**

17 **[6]University of Maryland Baltimore County, Baltimore, MD, USA**

18 **[7]Science Systems and Applications, Inc., Lanham, MD, USA**

19 **[8]Science and Technology Corporation, Madison, Wisconsin, 53703, USA**

20 **[9]Royal Belgian Institute for Space Aeronomy (BIRA-IASB), 1180 Brussels, Belgium**

21 **[10]Laboratoire Inter-universitaire des Systèmes Atmosphériques (LISA), UMR7583,**
22 **Universités Paris-Est Créteil et Paris, Diderot, CNRS, Créteil, FR**

23 **[11]Technische Universität München (TUM), School of Engineering and design, and**
24 **Deutsches Zentrum für Luft- und Raumfahrt (DLR), Institut für Methodik der**
25 **Fernerkundung (IMF), Oberpfaffenhofen, Germany**

26 **[12]Royal Netherlands Meteorological Institute, De Bilt, 3731 GA, the Netherlands**

27 **[13]Faculty of Civil Engineering and Geosciences, University of Technology Delft, Delft, 2628**
28 **CN, the Netherlands**

29 **[#]Now at University Savoie Mont Blanc, INRAE, CARRTEL, F-74200 Thonon-les-Bains,**
30 **France**

31 ***Correspondence: audrey.gaudel@noaa.gov**

32

Abstract

Tropical tropospheric ozone (TTO) is important for the global radiation budget because the longwave radiative effect of tropospheric ozone is higher in the tropics than mid-latitudes. In recent decades the TTO burden has increased, partly due to the ongoing shift of ozone precursor emissions from mid-latitude regions toward the equator. In this study, we assess the distribution and trends of TTO using ozone profiles measured by high quality in situ instruments from the IAGOS (In-Service Aircraft for a Global Observing System) commercial aircraft, the SHADOZ (Southern Hemisphere ADditional OZonesondes) network, and the ATom (Atmospheric Tomographic Mission) aircraft campaign, as well as six satellite records reporting tropical tropospheric column ozone (TTCO): TROPOMI, OMI, OMI/MLS, OMPS/MERRA2, CrIS, and IASI/GOME2. With greater availability of ozone profiles across the tropics we can now demonstrate that tropical India is among the most polluted regions (e.g., Western Africa, tropical South Atlantic, Southeast Asia, Malaysia/Indonesia) with present-day 95th percentile ozone values reaching 80 nmol mol^{-1} in the lower free troposphere, comparable to mid-latitude regions such as Northeast China/Korea. In situ observations show that TTO increased between 1994 and 2019, with the largest mid- and upper tropospheric increases above India, Southeast Asia and Malaysia/Indonesia (from 3.4 ± 0.8 to 6.8 ± 1.8 nmol mol^{-1} decade^{-1}), reaching 11 ± 2.4 and 8 ± 0.8 nmol mol^{-1} decade^{-1} close to the surface (India and Malaysia/Indonesia, respectively). The longest continuous satellite records only span 2004-2019, but also show increasing ozone across the tropics when their full sampling is considered, with maximum trends over Southeast Asia of 2.31 ± 1.34 nmol mol^{-1} decade^{-1} (OMI) and 1.69 ± 0.89 nmol mol^{-1} decade^{-1} (OMI/MLS). In general, the sparsely sampled aircraft and ozonesonde records do not detect the 2004-2019 ozone increase, which could be due to the genuine trends on this timescale being masked by the additional uncertainty resulting from sparse sampling. The fact that the sign of the trends detected with satellite records changes above three IAGOS regions, when their sampling frequency is limited to that of the in situ observations, demonstrates the limitations of sparse in situ sampling strategies. This study exposes the need to maintain and develop high frequency continuous observations (in situ and remote sensing) above the tropical Pacific Ocean, the Indian Ocean, Western Africa and South Asia in order to estimate accurate and precise ozone trends for these regions. In contrast, Southeast Asia and Malaysia/Indonesia are regions with such strong increases of ozone that the current in situ sampling frequency is adequate to detect the trends on a relatively short 15-year time scale.

Plain Language Summary

Tropospheric ozone is an air pollutant and a climate forcer, and plays an important role in the global Earth's radiation budget, especially in the tropics. In recent decades, the tropical tropospheric ozone burden has increased, partly due to the ongoing shift of ozone precursor emissions from mid-latitudes toward the equator. In this study, we assess the changes in time of tropical tropospheric ozone using in situ ozone profiles measured by high quality instruments from commercial aircraft, ozonesondes and satellites. In situ observations show that tropical tropospheric ozone increased between 1994 and 2019, with the largest increases above India, Southeast Asia and Malaysia/Indonesia. The longest continuous satellite records of ozone only span 2004-2019, but show increasing ozone across the tropics, with maximum trends over

2

76 Southeast Asia. In general, the sparsely sampled aircraft and ozonesonde records do not detect
77 the 2004-2019 ozone increase, which could be due to sample sizes that are too small for accurate
78 trend detection on this relatively short 15-year time period. The fact that the satellite records also
79 fail to consistently detect positive trends when their sampling frequency is limited to that of the
80 in situ observations demonstrates the limitations of sparse in situ sampling in the tropics. This
81 study demonstrates the need to maintain and develop continuous observations (in situ and remote
82 sensing) above the tropical Pacific Ocean, the Indian Ocean, Western Africa and South Asia in
83 order to estimate accurate and precise ozone trends for these regions.

84

85 **Short Summary (500 characters)**
86 The study examines tropical tropospheric ozone changes. In situ data from 1994-2019 display
87 increased ozone, notably over India, Southeast Asia, and Malaysia/Indonesia. Sparse in situ data
88 limit trend detection for the 15-year period. In situ and satellite data, with limited sampling,
89 struggle to consistently detect trends. Continuous observations are vital over the tropical Pacific
90 Ocean, Indian Ocean, Western Africa, and South Asia for accurate ozone trend estimation in
91 these regions.
92
93
94
95
96
97

98 **1. Introduction**
99   Tropospheric ozone negatively affects human health and vegetation, and it is a short-lived
100 climate forcer (Fleming et al., 2018; Mills et al., 2018; Gulev et al., 2022; Szopa et al., 2022).
101 The longwave radiative effect of tropospheric ozone is higher in the tropics and subtropics
102 (between 30˚S and 30˚N) compared to mid-latitudes (Doniki et al., 2015; Gaudel et al., 2018).
103 The most recent IPCC assessment concluded with a high level of confidence that tropical ozone
104 increased by 2-17% per decade in the lower troposphere, and by 2-12% per decade in the free
105 troposphere from the mid-1990s to the period 2015-2018 (Gulev et al., 2021). These increases
106 are especially strong across southern Asia (Gaudel et al., 2020), and according to the longest
107 available satellite record, ozone increases in this region have been occurring since at least 1979
108 (Ziemke et al., 2019). A comprehensive NASA analysis used the OMI/MLS satellite record to
109 show a clear increase of tropospheric column ozone (1-2.5 DU decade^{-1}) between 2005 and 2016
110 throughout the tropics, with larger trends over the Arabian Peninsula, India and Southeast Asia,
111 generally consistent with a simulation by NASA's MERRA-2 GMI global atmospheric
112 chemistry model (Ziemke et al., 2019). Similar results were found in a recent study using the
113 NASA Goddard Earth Observing System Chemistry Climate Model (Liu et al., 2022). Weak to
114 moderate positive trends of 0.6 and 1.5 nmol mol^{-1} decade^{-1} between 1995 and 2015-2018 were
115 also reported at two remote tropical surface sites (Mauna Loa, Hawaii, and American Samoa,
116 South Pacific; Cooper et al., 2020). A recent analysis of 1998-2019 tropical ozone trends using
117 the Southern Hemisphere ADditional OZonesondes (SHADOZ) network reported highly

118 seasonal but overall weak positive trends (1-2% decade^{-1}) in the mid-troposphere (5-10 km)
119 (Thompson et al., 2021).
120   Simulations by a wide range of global atmospheric chemistry models show that global-
121 scale increases of tropospheric ozone since pre-industrial times are driven by anthropogenic
122 emissions of ozone precursor gases (Archibald et al., 2020; Skeie et al., 2020; Griffiths et al.,
123 2021; Szopa et al., 2021; Wang et al., 2022; Fiore et al. 2022), with approximately 54% of the
124 1850-2000 global tropospheric ozone increase occurring in the tropics and subtropics (30° S –
125 30° N) (Young et al., 2013). A key ozone precursor that drives the background increase of
126 tropospheric ozone, especially in the free troposphere is methane (Thompson and Cicerone,
127 1986a,b; Hogan et al., 1991; Fiore et al., 2002). From 1980 to 2010 the estimated increase of the
128 global tropospheric ozone burden due to the increase of anthropogenic emissions and the partial
129 shift of the emissions from mid-latitudes towards the equator was 28.12 Tg (8.9%), with the
130 increase of methane (15%) accounting for one quarter of the ozone burden increase (as simulated
131 by the CAM-chem model; Zhang et al., 2016). Most of the ozone burden increase (64%)
132 occurred in the tropics and subtropics (30° S – 30° N), driven by emissions from South Asia,
133 Southeast Asia and by increasing background methane levels (Zhang et al., 2021). Similar rates
134 of ozone burden increases, peaking in the tropics, are simulated by a range of CMIP6 models
135 (1995-2014) (Skeie et al., 2020,) the GEOS-Chem model (1995-2017) (Wang et al., 2022), the
136 JPL TCR-2 chemical reanalysis (1995-2018) (Miyazaki et al., 2020), and a 15-member initial-
137 condition ensemble generated from the CESM2-WACCM6 chemistry-climate model (1950-
138 2014) (Fiore et al., 2022). The increase of methane has continued to the present and the observed
139 global mean methane increase from 1983 to 2023 is 18% (the increase is 8% since 2004 when
140 the OMI satellite instrument began operations) (www.gml.noaa.gov). Under a future scenario of
141 high anthropogenic emissions and continuously increasing methane concentrations (Griffiths et
142 al., 2021), the global ozone burden is expected to increase for the remainder of the 21st century
143 (see the ssp370 scenario in Figure 6.4 of Szopa et al., 2021), with increases of approximately
144 10% from 2014 to 2050. In the tropics the strongest increases (though 2050) are expected across
145 South Asia (10-20%), with little or no increase across the remote regions of the equatorial Pacific
146 and equatorial Atlantic.
147   The tropics are characterized by high ozone values over the southern tropical Atlantic and
148 Southeast Asia (Fishman et al., 1990; Fishman et al., 1996; Thompson et al., 1996; Logan et al.,
149 1999; Ziemke et al., 2019) and low ozone values (< 10 nmol mol^{-1}) in the free troposphere over
150 the Pacific warm pool (Kley et al., 1996), although these low values have become less frequent
151 over the last two decades (Gaudel et al., 2020). The spatial distribution of tropical tropospheric
152 ozone (TTO) can vary on a range of timescales. On multi-year timescales TTO experiences a
153 dipole oscillation across the tropical Pacific Ocean due to El Niño-Southern Oscillation (ENSO)
154 (Chandra et al., 1998; Doherty et al., 2006; Oman et al., 2013; Xue et al., 2020). On seasonal
155 time scales ozone can vary with the Madden-Julian Oscillation (MJO) (Ziemke et al., 2015), and
156 also with dry and wet conditions (a.k.a. biomass burning and monsoon seasons) related to the
157 seasonal shifts of the Intertropical Convergence Zone (ITCZ) (Fishman et al., 1992; Oltmans et
158 al., 2001; Sauvage et al., 2007; Thompson et al., 2012). In a given season, TTO can be further
159 influenced by biomass burning, lightning, inter-hemispheric transport and stratospheric
160 intrusions/large-scale subsidence (Sauvage et al., 2007; Jenkins et al., 2014; Yamasoe et al.,

2015; Hubert et al., 2021). For instance, high ozone concentrations were recently measured above the tropical Atlantic (Bourgeois et al., 2020), and were attributed to biomass burning emissions, whose effects on tropospheric ozone enhancements are underestimated by global chemistry-transport models, especially in the tropics and the southern hemisphere (Bourgeois et al., 2021).

While decades of research on the distribution of TTO using satellite instruments (Fishman et al., 1986, 1987, 1990; Ziemke et al., 1998, 2005, 2009, 2011, 2019) and in situ observations (Logan et al., 1999; Thompson et al., 2000, 2003, 2012, 2021; Oltmans et al., 2001; Sauvage et al., 2005; Sauvage et al., 2007; Yamasoe et al., 2015; Tarasick et al., 2019; Cooper et al., 2020, Lannuque et al., 2021) have characterized the spatial and temporal variability of TTO concentrations, reconciling differences between satellite and in situ observations has been a challenge (Gaudel et al., 2018).

To update our understanding of tropospheric ozone's distribution and trends across the tropics, this study presents a quantitative analysis of four complementary data sets in time and space across the 20˚S-20˚N latitude band: (1) Thousands of vertical ozone profiles from the In-Service Aircraft for a Global Observing System (IAGOS) (Nédélec et al., 2015; Blot et al., 2021) above five continental regions; (2) Regular vertical profiles from the SHADOZ ozonesonde network (Thompson et al., 2017; Stauffer et al._, 2022) above 14 continental and oceanic sites; (3) Vertical profiles from the Atmospheric Tomographic Mission (ATom) aircraft campaign above five oceanic regions; (4) Tropospheric column ozone retrievals from four well-known and two new satellite records.

The paper is organized as follows. Section 2 describes the data sets and the methodology for quantifying the distribution and trends of ozone. Section 3 presents the results that include the distribution of ozone from the in situ data, an evaluation of the satellite records and the trend estimates from IAGOS, SHADOZ and satellite records. Section 4 presents the main conclusions.

2. Methods

We define the tropics as the latitude band between 20˚S and 20˚N, within the bounds of the Tropic of Cancer and the Tropic of Capricorn. This latitude band covers most of the Southern Hemisphere ADditional OZonesondes (SHADOZ) network designed to measure ozone in the subtropics/tropics. The goal of the study is to characterize the 20˚S-20˚N latitude band that can be impacted by subtropical air masses in some regions, especially at the edge of the domain. The satellite data are shown for the same latitude domain.

We focus on three time periods: 2014-2019, also called "present-day" to assess the distribution of TTO (5th, 50th, and 95th percentiles) with in situ data above the sampled regions and sites described in Figure 1; 1994-2019 to assess ozone trends using in situ data records for more than two decades; 2004-2019 to assess ozone trends over the time period of the Ozone Monitoring Instrument (OMI) data set, which is the longest time series of ozone measured from space from a satellite.
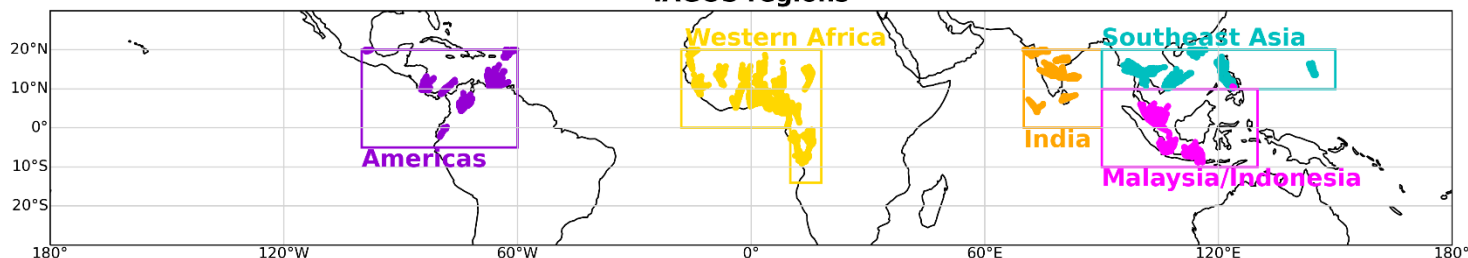
We also use new datasets to assess the distribution of TTO, such as the ATom aircraft campaign, and the CrIS and IASI/GOME2 satellite records.

2.1 In situ measurements

204

205
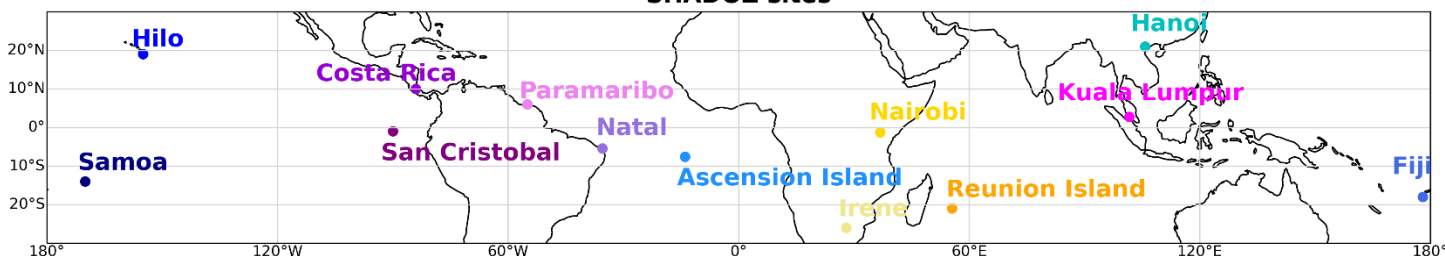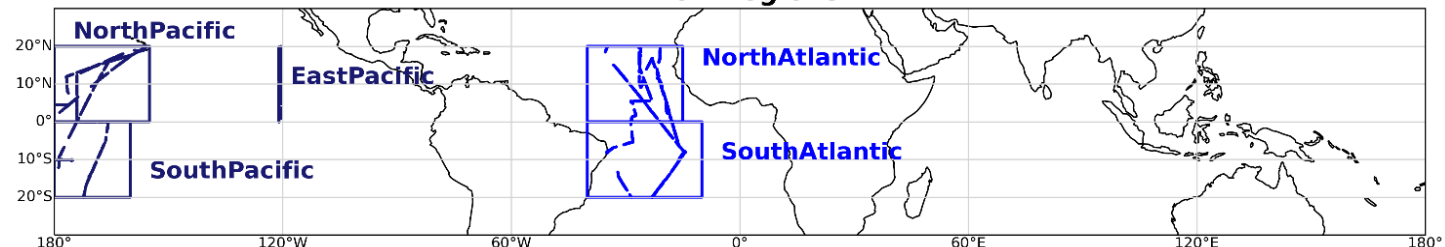
206

207

208

209

210

211 **Figure 1**. Regions and sites of IAGOS, SHADOZ and ATom measurements used in this study to
212 assess the 5th, 50th and 95th percentiles of ozone in the tropical troposphere over 2014-2019. Data
213 from IAGOS and ATom flights are clustered into specific regions such as Americas, Western
214 Africa, India, Southeast Asia, Malaysia/Indonesia, North Pacific, South Pacific, East Pacific,
215 North Atlantic and South Atlantic. IAGOS and ATom flight tracks are plotted on the map to
216 show the specific sampling locations for 2014-2019. IAGOS and SHADOZ data are statistically
217 fused above the Americas, Southeast Asia and Malaysia/Indonesia and used to estimate ozone
218 trends between 1994 and 2019. For India, only IAGOS data are available for the ozone trend
219 estimate between 1994 and 2019.

220

221 **2.1.1 IAGOS**
222   Description: The European research infrastructure In-service Aircraft for a Global
223 Observing System (IAGOS), formerly known as the Measurement of Ozone and Water Vapor by
224 Airbus In Service Aircraft (MOZAIC), has collected continuous high quality ozone profiles up to
225 12 km (~ 200 hPa) on-board commercial aircraft since 1994 (Blot et al., 2020). Ozone is

226 measured using a UV analyzer (Thermo Scientific, model 49) and the total uncertainty is ±2
227 nmol mol^{-1} ±2% (Nédélec et al., 2015).
228   Data treatment: For this study, we consider five tropical regions: Americas, Africa, India,
229 Southeast Asia and Malaysia/Indonesia. We use IAGOS data to assess the average ozone
230 distribution between 2014 and 2019, referred to as "present-day ozone", as well as to assess
231 ozone trends between 1994 and 2019. Over the time period 1994-2019, the most frequented
232 airports were Caracas (1214 profiles) and Bogota (560 profiles) for the Americas; Lagos (761
233 profiles) and other airports in the Gulf of Guinea for Western Africa; Chennai (680 profiles) and
234 Hyderabad (552 profiles) for India; Bangkok (1535 profiles) and Ho Chi Minh City (367
235 profiles) for Southeast Asia; Singapore (265 profiles), Kuala Lumpur (208 profiles) and Jakarta
236 (113 profiles) for Malaysia/Indonesia (Table S1). All available ozone profiles from these airports
237 are used in this study. The individual ozone profiles are averaged to a common vertical
238 resolution of 10 hPa prior to any further analysis. To assess the annual ozone distribution the
239 profiles are averaged annually. To assess ozone trends, the quantile regression method is applied
240 to individual profiles (section 2.5). To compare with the satellite data, the profiles were averaged
241 monthly before being converted to a tropospheric column value ranging from the surface up to
242 270 hPa or up to the maximum altitude (~ 200 hPa). We chose 270 hPa to be consistent with the
243 TROPOMI tropical tropospheric column ozone. While some of the satellite records used in this
244 study have an upper limit at 150 hPa (thermal tropopause), IAGOS commercial aircraft do not
245 reach these altitudes.
246
247 **2.1.2 SHADOZ**
248   Description: The Southern Hemisphere ADditional OZonesondes (SHADOZ) network
249 has provided ozone profiles at multiple sites between 25ºS and 21ºN since 1998, and presently
250 operates 14 sites. SHADOZ is a NASA-sponsored project operated by NOAA and 15 institutions
251 around the world (Thompson et al., 2003a, 2003b, 2012, 2021). The SHADOZ archive of ozone
252 profiles, measured by electrochemical concentration cell (ECC) ozonesondes, were reprocessed
253 in 2016-2018 (Witte et al., 2017; 2018). In comparisons of the reprocessed data with collocated
254 total ozone spectrometers and satellite overpasses, the reprocessed SHADOZ total ozone column
255 (TOC) disagreed with the independent data within 2% (Thompson et al., 2017). SHADOZ data
256 since 2018 have been collected and processed according to the same protocols as the reprocessed
257 profiles (Stauffer et al., 2018, 2020; 2022; WMO/GAW 268, 2021). A recent study of TOC
258 stability over 60 global stations revealed an artifact of declining tropospheric ozone at the
259 SHADOZ Hilo and Costa Rican stations (Stauffer et al., 2020; 2022). Those data were not used
260 in the recent Thompson et al. (2021) study that showed distinctive seasonal and regional
261 variations in ozone trends collected at eight SHADOZ stations within ±15º latitude of the
262 equator.
263   Data treatment: As with the IAGOS data, the SHADOZ ozone profiles were averaged to
264 a common vertical resolution of 10 hPa before any further analysis. The 10 hPa-resolution
265 vertical profiles are fused with the IAGOS 10 hPa-resolution vertical profiles to assess trends
266 between the surface and 200 hPa (section 2.6). To compare with the satellite data, the profiles
267 were averaged monthly before being converted to tropospheric columns up to 270 hPa, 150 hPa
268 and 100 hPa.

269
2.1.3 ATom
270

Description: The Atmospheric Tomography (ATom) project was a global scale NASA aircraft mission which collected profiles of ozone and hundreds of other atmospheric constituents in remote regions above the Atlantic and Pacific basins on board the NASA DC-8 aircraft. The project consisted of four seasonal circumnavigations of the globe, one in each season, continually profiling the troposphere between 180 m and 14 km above sea level (a.s.l.) with a temporal resolution of 10 Hz, averaged to 1 Hz (data available at https://espo.nasa.gov/atom, last access March 7, 2022). The ATom mission occurred in July–August 2016 (ATom-1), January–February 2017 (ATom-2), September– October 2017 (ATom-3), and April–May 2018 (ATom-4). Ozone was measured using the National Oceanic and Atmospheric Administration (NOAA) nitrogen oxides and ozone (NOyO3) instrument (Bourgeois et al. 2020). The total estimated uncertainty at sea level is $\pm$ (0.015 nmol mol^{-1} $\pm$ 2 %).

Data treatment: We used the ATom ozone profiles available above five regions in the tropics: North Pacific, South Pacific, East Pacific, North Atlantic and South Atlantic. Most of the regions were sampled over one day in August 2016, February and October 2017, and May 2018, except the East Pacific which was sampled in July 2016, January and September 2017, and April 2018. Each flight produced 6-14 profiles in each region. Therefore, the ATom dataset is used to assess the ozone distribution over the 2016-2018 time-period and for the annual comparison with the satellite products. As for IAGOS and SHADOZ, we averaged the profiles to a common vertical resolution of 10 hPa within the five ATom regions. To compare with satellite data, the profiles were converted to tropospheric column ozone from the near-surface measurements up to 270 hPa and averaged for the entire ATom period above each of the five regions.

2.2 Tropical Tropospheric Column Ozone (TTCO) estimation from IAGOS, SHADOZ and ATom

In this study and as mentioned in Section 2.1, the ozone profiles from in situ observations have been converted to columns to evaluate the satellite products. The current TOAR-II Harmonization and Evaluation of Ground-based Instrument for Free Tropospheric Ozone Measurements (HEGIFTOM) focus working group (https://hegiftom.meteo.be/) recommended 150 hPa as the top limit of the TTCO in the 15˚S-15˚N tropical band and 200 hPa in the 15˚S-30˚S/15˚N-30˚N bands. As we focus our study on the 20˚S-20˚N latitude band, we decided to use the 150 hPa top limit. Some variations on the TTCO definition occur in this study and are detailed below, but are not corrected for.

IAGOS aircraft cannot reach 150 hPa as they have a maximum cruise altitude around 200 hPa. Therefore, only SHADOZ ozonesondes, which reach the mid- or upper stratosphere, were used to calculate TTCO from the surface to 150 hPa. However, we additionally calculated TTCO up to 270 hPa with IAGOS and ATom to compare with TROPOspheric Monitoring Instrument (TROPOMI) and Infrared Atmospheric Sounding Interferometer (IASI) / Global Ozone Monitoring Experiment 2 (GOME2) satellite data.

2.3 Satellite data

In this study we mainly focus on satellite data based on ultraviolet absorption (UV) retrievals, supplemented with two ozone records derived from infrared (IR) measurements as described below. Two key parameters differ between the satellite datasets: (i) the top limit used to define the tropospheric column ozone, and (ii) the horizontal coverage. Figure S1 shows the time series of the pressure level characterizing the top limit. Depending on the datasets, the top limit is constant or varies with time. The tropical coverage is 20˚S-20˚N for all satellite records. All satellite records were averaged to a common 5˚x5˚ monthly grid.

2.3.1 TROPOMI CCD

The TROPOspheric Monitoring Instrument (TROPOMI, Veefkind et al., 2012) was launched onboard the Sentinel-5 Precursor (S5P) satellite in October 2017. The tropospheric column ozone data from TROPOMI, inferred using the convective cloud differential technique (CCD, Ziemke et al., 1998; Heue et al., 2016; Hubert et al., 2021), covers the 20˚S-20˚N latitude band, between the surface and 270 hPa. For this study, we compute monthly data from daily measurements on a 5˚ x 5˚ grid to be consistent with the other satellite data records. For the 5˚ x 5˚ gridded data we estimate the uncertainty of the TROPOMI CCD tropospheric ozone column to be about 2 DU. We only use data from 2019, which is the last year of our present-day time period 2014-2019.

2.3.2 OMI CCD

The Ozone Monitoring Instrument (OMI) was launched onboard the Aura satellite in July 2004. For this study we used tropical tropospheric column ozone retrieved using the CCD technique (Ziemke et al., 1998; Ziemke and Chandra, 2012), which is consistent with TROPOMI-derived TTCO. The tropospheric column is defined between the surface and 100 hPa, and it covers the 20˚S-20˚N latitude band inherent to the CCD technique. OMI records are available since 2004 and for this study we use monthly means to assess ozone distribution during the present-day time period of 2014-2019 as well as the trends of ozone over 2004-2019. The monthly accuracy and precision (1σ) are 3 and 3.5 DU, respectively.

2.3.3 OMI/MLS

The OMI and the Microwave Limb Sounder (MLS) sensors are both onboard the Aura satellite and the tropospheric column ozone is retrieved by subtracting the stratospheric column ozone measured by MLS from the total column ozone measured by OMI (Ziemke et al., 2006). The top limit of the OMI/MLS tropospheric column ozone is the thermal tropopause calculated from NCEP reanalysis data using the World Meteorological Organization (WMO) 2 K km^{-1} lapse-rate definition. The tropopause varies seasonally between 95 and 115 hPa (Figure S1). OMI/MLS data cover the 60˚S-60˚N latitude band and for this study we focus on the 20˚S-20˚N latitude band. The monthly accuracy and precision (1σ) are 2 and 1.5 DU, respectively. Further details of the OMI/MLS product and a description of an updated drift correction can be found in Section S.4 of the supplementary material.

2.3.4 OMPS/MERRA2

354   The Ozone Mapping Profiler Suite (OMPS) was launched in January 2012 onboard the
355 Suomi National Polar-orbiting Partnership (Suomi NPP) spacecraft. The tropospheric column
356 ozone is retrieved by subtracting the stratospheric column of MERRA2 (Modern-Era
357 Retrospective analysis for Research and Applications, version 2) ozone reanalysis data from the
358 total column ozone of the OMPS nadir mapper (Ziemke et al., 2019). The derived daily
359 tropospheric column ozone uses the MERRA2 tropopause with assimilated MLS ozone. The
360 MERRA2 tropopause was determined using a potential vorticity (PV) – potential temperature (θ)
361 definition (2.5 PV units, 380 K; Wargan et al., 2020). The tropopause at a given grid point was
362 taken as the larger of these two PV and θ surfaces. However, in this study, the tropopause is
363 exclusively defined by θ surfaces as we focus on the 20˚S-20˚N latitude band. For the MERRA2
364 assimilation, in 2015 MLS changed from version 2.2 to version 4.2 (Wargan et al., 2017; Davis
365 et al., 2017). This produced a 1-1.5 DU difference between the earlier and latter record for
366 stratospheric column ozone, which prevents accurate trend detection from either MERRA2
367 stratospheric column ozone or the derived tropospheric column ozone from OMPS/MERRA2.
368 The OMPS/MERRA 2 tropopause pressure varies seasonally between 95 hPa and 108 hPa
369 (Figure S1). The monthly accuracy and precision (1σ) are 3 and 2 DU, respectively.
370

2.3.5 CrIS

372   The Cross track Infrared Sounder (CrIS) is onboard the Suomi NPP (2011–2021) and
373 JPSS-1 (NOAA-20 in operations; 2017–present) and builds upon the hyperspectral IR record
374 first started by the Atmospheric Infrared Sounder (AIRS) on Aqua (2002–2022). For this study
375 we are focusing on the ozone profiles retrieved by the Community Long-term Infrared
376 Microwave Combined Atmospheric Product System (CLIMCAPS, Smith and Barnet, 2019;
377 2020). CLIMCAPS retrieves atmospheric state parameters, including ozone profiles (from the
378 surface to the top of the atmosphere), from AIRS and CrIS to form a long-term record that spans
379 instrument and platform differences. CLIMCAPS uses MERRA2 as the a-priori for ozone. Here
380 we focus on CLIMCAPS from CrIS onboard Suomi NPP (National Polar-orbiting Partnership,
381 2016-01-01 to 2018-03-31) and NOAA-20 (previously known as JPSS-1, 2018-04-01 to 2022-
382 08-31) for the time period 2016-2019 because this gives us the baseline IR sounding capability
383 for the next two decades (CrIS is scheduled for launch on three additional JPSS platforms). CrIS
384 data covers the 90˚S-90˚N latitude band and for this study we focus on the 20˚S-20˚N latitude
385 band. The accuracy of CrIS tropospheric ozone data varies between -9.4% globally and -20% in
386 the tropics compared with ozonesondes. The precision is 21.2% globally (Nalli et al., 2017).
387   For CrIS, we accessed CLIMCAPS Level 2 retrievals via NASA GES DISC (NASA
388 Goddard Earth Sciences Data and Information Services Center; Sounder SIPS, & Barnet, Chris.,
389 2020a and 2020b; https://disc.gsfc.nasa.gov/). We aggregated them onto 1˚ equal angle global
390 grids. Specifically, we accessed the ozone retrieved fields (o3_mol_lay) defined as 100 layer
391 column density profiles [molec m^{-2}] and subset them into tropospheric profiles. We defined the
392 troposphere as all values between Earth surface (prior_surf_pres) and tropopause (tpause_pres).
393 A total column value is simply the sum of all column density values, converted to DU. We used
394 the quality flag (ispare_2=0) to define all successful retrievals, which we simply averaged per
395 grid box. No other filtering was done. CLIMCAPS retrievals are done from cloud cleared
396 radiances so we do not have to make specific accommodation for clouds.
397

2.3.6 IASI / GOME2

IASI/GOME2 is a multispectral approach used to retrieve ozone for several partial columns. It is based on the synergism of IASI and GOME-2 measurements respectively in the thermal infrared and the ultraviolet spectral domain, jointly used in terms of radiance spectra for enhancing the sensitivity of the retrieval for lowermost tropospheric ozone (below 3 km above sea level, see Cuesta et al., 2013). Studies over Europe and East Asia have shown good skill for capturing near surface ozone variability compared to surface in situ measurements of ozone (Cuesta et al. 2018; 2022). This ozone product offers global coverage for low cloud fraction conditions (below 30%) for 12-km diameter pixels spaced by 25 km (at nadir pointing). The IASI/GOME2 global dataset is publicly available through the AERIS French data center, with data from 2017 to the present (available at https://iasi.aeris-data.fr/o3_iago2/, last accessed 08/02/2023) and covers the 90˚S-90˚N latitude band. For this study, we are using the 2017-2021 monthly tropospheric column ozone between the surface and 12 km, focusing on the 20˚S-20˚N latitude band.

2.4 Comparison between satellite and in situ data

To assess the performance of the six satellite records, we calculated the mean biases between satellite-detected monthly TTCO and IAGOS and SHADOZ integrated profiles over the 2014-2019 time period. The biases are calculated as follows:

$$\text{Mean Bias (MB in DU)} = \frac{\sum_{i=1}^{N} y_{i(sat)} - y_{i(ref)}}{N}$$

$$\text{Normalized Mean Bias (NMB in \%)} = \frac{1}{N} \sum_{i=1}^{N} \frac{y_{i(sat)} - y_{i(ref)}}{y_{i(ref)}} \times 100$$

N is the number of monthly TTCO observations over a given region/site and y_i is the monthly mean TTCO based on in situ data (ref) or satellite data (sat).

In order to represent the relationship between the satellite data and the in situ data, we used a least-square linear regression as well as the orthogonal distance regression (ODR). In this exercise, we are not using strict sampling criteria in time and space (except for the satellite and in-situ observations being in the same month, year and grid cell), nor smoothing in situ ozone profiles to the vertical resolution of the satellite data before integration. To extract satellite data over IAGOS and ATom regions, we used a 5˚x5˚ gridded mask reflecting monthly grid cells with available IAGOS and ATom data, and only these grids are used to compute regional mean satellite values. For comparison to SHADOZ data, satellite data were extracted at the latitude and longitude of the SHADOZ sites (sonde launch site within satellite pixel). We include all satellite records with a minimum of one year of data within 2014-2019.

2.5 Fused product and trend estimation

The tropical region has sparse in situ sampling in both time and space, which makes accurate quantification of trends challenging. Based on a sampling sensitivity test (sections S1, S2, Figures S2 and S3), we conclude that one profile per week is only sufficient for detection of

trends with a very strong magnitude (i.e., > |3| nmol mol^{-1} decade^{-1}), which is not common in the free troposphere. We show that a sampling frequency of 7 profiles per month is sufficient for basic trend detection (i.e., to reliably determine if there is a trend) of TTO using the datasets presently available (if the magnitude of a trend is greater than |1| nmol mol^{-1} decade^{-1}), but additional data are required for accurate quantification or detection of a weaker trend.

Because the sparse sampling makes trend detection difficult, we have chosen to statistically fuse the in situ measurements from the IAGOS and SHADOZ programs over large regions, which includes air masses from different origins and influences (Figures 1 and S12 to S16). The method is based on a data fusion technique described by Chang et al. (2022), which considers ozone correlation structure, sampling frequency and inherent data uncertainty. By investigating systematic ozone variability, the resulting fused product allows us to reconcile the differences between heterogeneous datasets and enhance the detectability of trends. For the Americas, we fused SHADOZ data over San Cristobal and Paramaribo with the IAGOS data (Figure S12); for Southeast Asia, we fused SHADOZ over Hanoi with the IAGOS data (Figure S13); for Malaysia/Indonesia, we fused SHADOZ data over Kuala Lumpur and Watukosek (Java) with the IAGOS data (Figure S14). For Western Africa and India, SHADOZ data are not available and we show the timeseries of just the IAGOS data in Figure S15 and S16, respectively.

For IAGOS data and the fused product, the trend estimate and its associated uncertainty are based on quantile regression (Koenker & Hallock, 2001), which is an appropriate choice for ozone profile time series, because of the irregular sampling schemes and the need to evaluate ozone changes associated with a range of percentiles (Chang et al., 2021). Data gaps are not interpolated as interpolation creates fictitious sample sizes for trend detection, while treating the missing data as not substantially deviant from the available data variability. Due to limited available sample sizes, only median trends (i.e., an estimate of the trend based on the median change in data distribution) are reported in this study. It should be noted that quantile regression is specifically designed to evaluate the distributional changes (determined by all available profiles). Although trends in extreme percentiles are not considered due to insufficient samples, by focusing on the median changes, our trend estimates are expected to be more robust against extreme variability or less impacted by potential large sampling bias (due to imbalanced sampling). The R and Python codes for implementing quantile/median regression are provided in the TOAR statistical guidance note (Chang et al., 2023). To account for potential correlation between ozone and climate variability, such as ENSO (El Niño-Southern Oscillation) and QBO (quasi-biennial oscillation), the trend model is specified through:

$$\text{anomaly} = b0 + b1\ \text{Trend} + b2\ \text{ENSO} + b3\ \text{QBO(30mb)} + b4\ \text{QBO(50mb)} + \text{Noise} \quad [1]$$

where b0 is the intercept, b1 is the linear trend, b2 is the regression coefficient for ENSO, b3 and b4 are coefficients for QBO at 30 and 50 mb, respectively. The trend uncertainty is derived by a bootstrapping method (Feng et al., 2011). The ENSO and QBO indexes can be found in the data availability section. Figure S17 shows that if ENSO and QBO are not considered, the trends can be offset by about 1-2 nmol mol^{-1} decade^{-1} at individual pressure layers over the five IAGOS regions, except Africa where the trend differences are negligible.

481   In addition, we conducted trend analysis of the monthly TTCO from SHADOZ, IAGOS,
482   OMI and OMI/MLS as well as the tropical ozone burden (TOB, Tg decade^{-1}) over zonal monthly
483   means using OMI and OMI/MLS. The OMI/MLS TTCO has shown a drift over time that we
484   corrected for this study (see section S4).

485

486   **3. Results**
487   **3.1 Ozone Profiles**

488
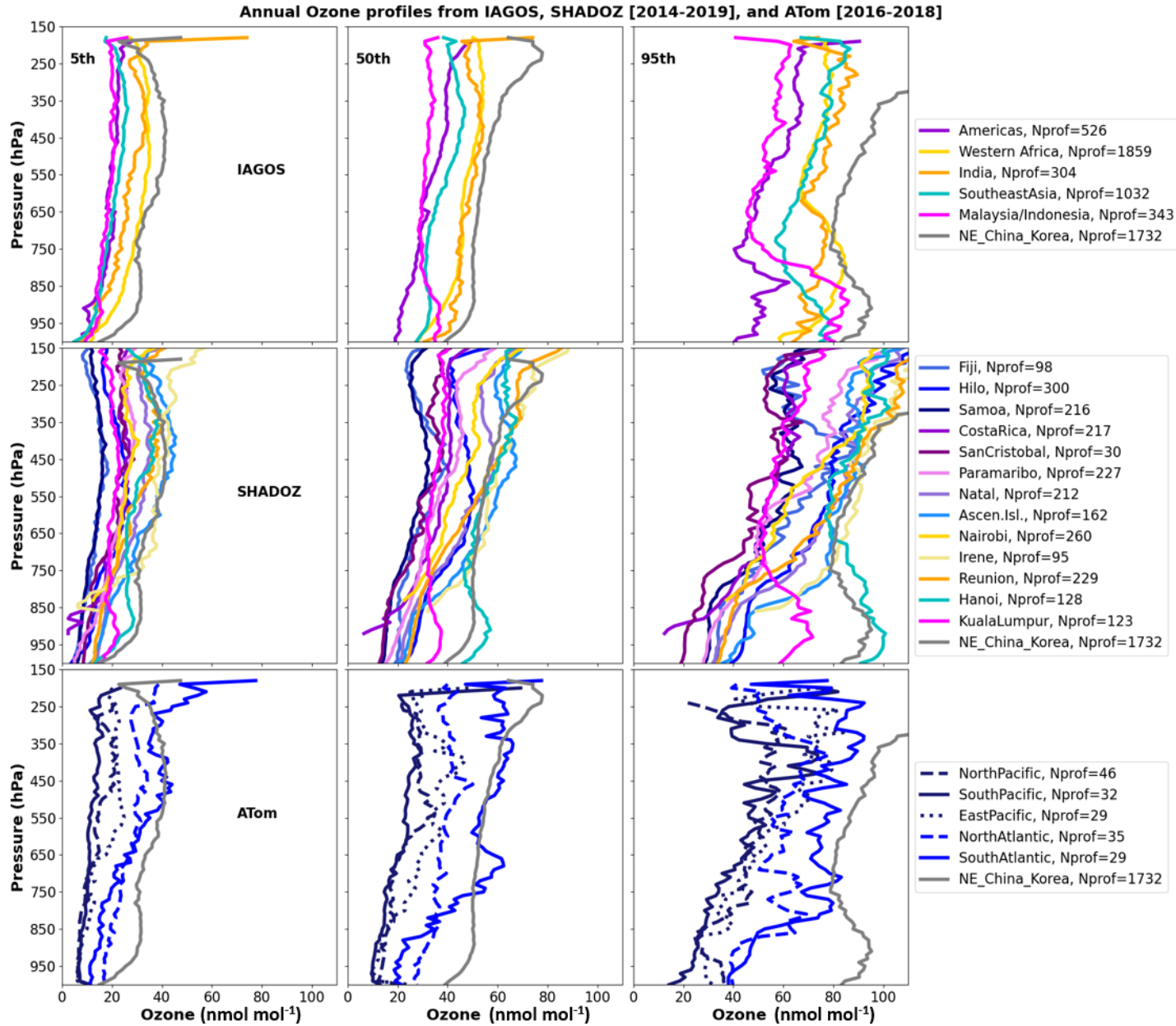
489
490   **Figure 2.** Distribution of tropical tropospheric ozone (TTO) showing annual 50th, 5th and 95th
491   percentiles (left, center, and right columns, respectively) of ozone profiles (nmol mol^{-1})
492   measured by IAGOS (top), SHADOZ (middle) both between 2014 and 2019, and ATom

496

497   For the period 2014-2019 (IAGOS, SHADOZ) and 2016-2018 (ATom), the three in situ
498 data sets show a range of ozone values from the surface to 200 hPa, indicative of the different
499 photochemical and transport regimes across the tropics (Figure 2). Here we highlight several
500 notable features.
501   The 50th and 95th percentiles of SHADOZ data over Hanoi (up to 100 nmol mol^{-1}) are
502 much higher than at the other sites/regions, especially below 750 hPa. Hanoi experiences strong
503 regional ozone production with a significant contribution from biomass burning in the Indochina
504 peninsula, especially in spring (Ogino et al., 2022).
505   Ozone levels are lowest above the tropical South Pacific (dark blue lines on the
506 SHADOZ and ATom panels of Figure 2) and the Americas (IAGOS: mostly represented by
507 measurements above Caracas and Bogota, and SHADOZ: San Cristobal, purple lines on both
508 panels of Figure 2), with the 5th percentile below 10 nmol mol-1, particularly in the lower
509 troposphere. These low ozone values are due to the ozone sink near the marine boundary layer
510 coupled with deep convection above the tropical South Pacific (Kley et al., 1996) and San
511 Cristobal (Oltmans et al., 1999). Above Caracas, the local influence is notable, with low ozone
512 levels observed during the wet season (May-December) (Yamasoe et al, 2015; Sanhueza et al.,
513 1999). Additionally, Seguel et al. (2024) report lower ozone exposure (MDA8 health metric) in
514 Bogota and Quito than in other South American sites, likely due to intense vertical mixing as
515 observed in Quito (Cazorla et al., 2021a; Cazorla, 2017).
516   The 95th percentile ozone is highest above Africa, India and Southeast Asia in the mid-
517 and upper troposphere, and above Southeast Asia and Malaysia/Indonesia in the boundary layer.
518 The tropical South Atlantic (ATom and Ascension Island) is also notable due to broad
519 enhancements from the lower free troposphere to the upper troposphere, with values of 60-80
520 nmol mol^{-1}. Similar patterns are seen in the median (50th percentile) ozone profiles, albeit with
521 lower mixing ratios.
522   As a frame of reference, we show the polluted mid-latitude region of Northeast China /
523 Korea from IAGOS data in 2014-2019, notable for its high ozone values (Gaudel et al., 2020). In
524 most cases the ozone profiles of Northeast China / Korea are similar to the maximum tropical
525 ozone profiles, but some regions exceed the Northeast China / Korea ozone values, such as
526 Southeast Asia / Hanoi, Southern Africa, and the tropical South Atlantic / Ascension Island.
527   Based on observations from the 1980s and 1990s, ozone levels in the tropics have
528 generally been considered to be lower than in the mid- and high latitude regions, with the
529 exception of the tropical Atlantic (Logan et al., 1999; Fishman et al., 1990). However, with
530 greater availability of ozone profiles across the tropics we can now demonstrate that tropical
531 India, Southeast Asia, and Malaysia/Indonesia are among the most polluted regions and are
532 comparable to the mid-latitude regions in terms of ozone pollution (Figure 2). We note that this
533 unique finding regarding India only pertains to the tropical regions as ozone enhancements
534 across northern India were detected by the TOMS/SBUV instruments as far back as 1979
535 (Gaudel et al., 2018).

536

537
538
539   **3.2 Tropical Tropospheric Column Ozone (TTCO)**
540
541
542
543
544
545
546
547
548
549
550
551
552

554
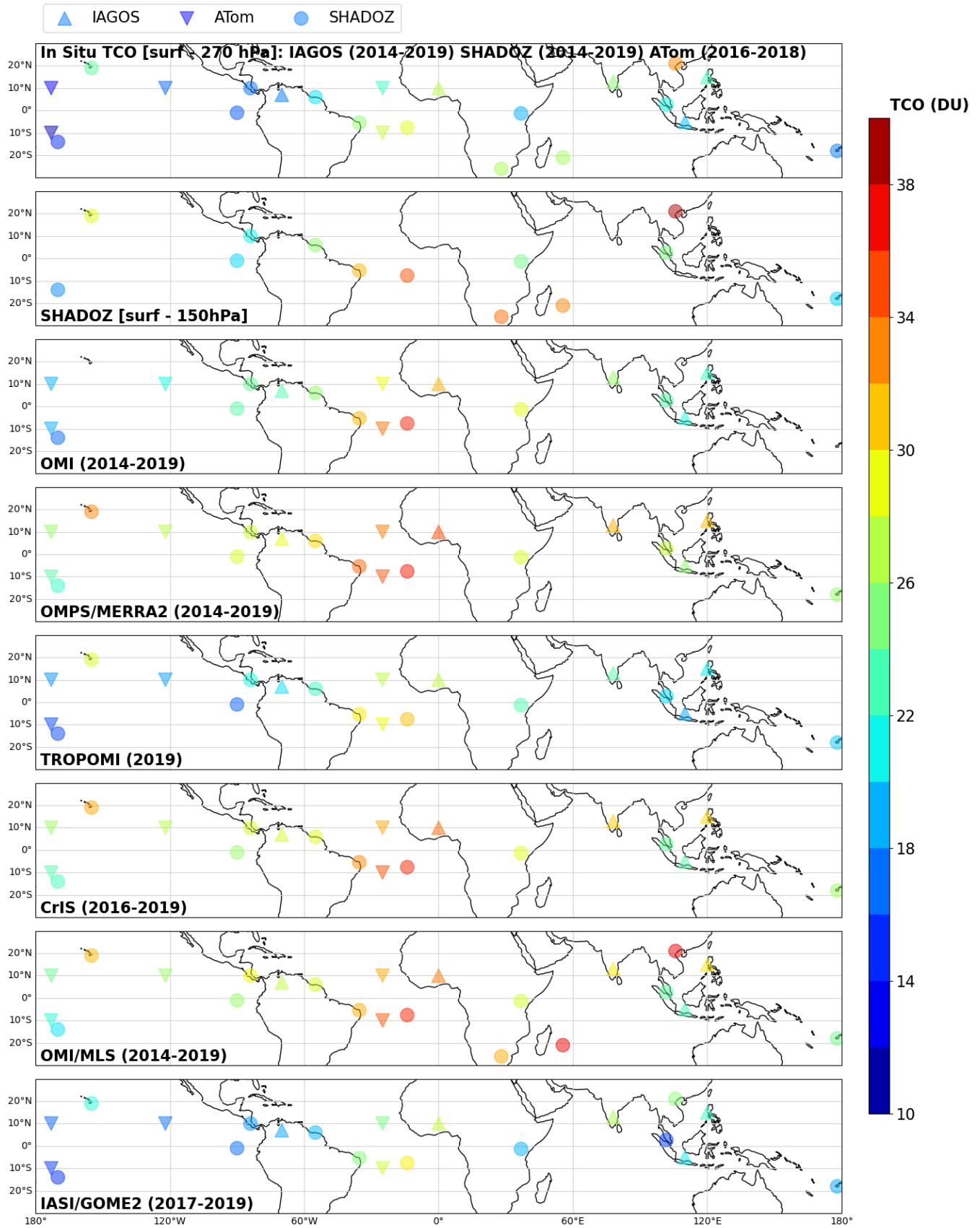
Figure 3. Annual tropical tropospheric column ozone (TTCO, surface-270 hPa) from in situ data
(IAGOS, SHADOZ between 2014 and 2019 and ATom between 2016 and 2018) (top panel),
TTCO (surface-150 hPa) from SHADOZ (2nd panel) between 2014 and 2019; and from OMI
(surface to 100 hPa, 2014-2019), OMPS/MERRA2 (surface to potential temperature at 380 K,
2014-2019), TROPOMI (surface to 270 hPa, 2019), CrIS (surface to 2016-2019), OMI/MLS
(surface to thermal tropopause, 2014-2019) and IASI/GOME2 (surface to 12 km, 2017-2019).

561
562

563   Figure 3 shows the tropical tropospheric column ozone (TTCO) for SHADOZ, IAGOS
564 and ATom and for the six-satellite records (OMI, OMPS/MERRA2, TROPOMI, CrIS,
565 OMI/MLS and IASI/GOME2). As mentioned in Section 2, we focus on the 2014-2019 time
566 period to study the TTCO distribution. However, ATom data are only available between 2016
567 and 2018, and some satellite records only cover one or two years within the five-year period we
568 have chosen. The in situ columns in Dobson units (DU) shown on the first panel of Figure 3 are
569 from the surface to 270 hPa, with ozone varying between 11 and 33 DU. When the TTCO is
570 calculated with profiles extending up to 150 hPa (2nd panel of Figure 3 with SHADOZ only),
571 ozone varies between 18 and 39 DU. As seen with the profiles (section 3.1), the minimum TTCO
572 values are observed over the Pacific Ocean and the maximum TTCO values are observed over
573 the Atlantic, Africa, India and Hanoi. The six-satellite records reproduce quite well the
574 variability of ozone with longitude. However, the range of TTCO values varies by product.
575 TTCO values under 20 DU are found over the Pacific Ocean with OMI CCD, TROPOMI and
576 IASI/GOME2, and over Southern Asia with IASI/GOME2. TTCO values above 30 DU are
577 found over the Atlantic Ocean with all satellite records except IASI/GOME2, and over Africa,
578 India and Southeast Asia with OMPS/MERRA2, CrIS and OMI/MLS.
579   Qualitatively, the mid- to upper tropospheric ozone maximum above the Atlantic and
580 Africa is well known (Fishman et al., 1987; Thompson et al., 2003) and explained by subsidence
581 of air masses rich in ozone (Krishnamurti et al., 1996; Thompson et al., 2000, 2003), emissions
582 of lightning NO_x ($LiNO_x$, Sauvage et al., 2007), emissions of CO/VOCs from biomass burning
583 (Ziemke et al., 2009; Bourgeois et al., 2021) and urban emissions (Tsivlidou et al., 2022). Hanoi,
584 at the northern edge of our domain, shows previously documented large ozone enhancements
585 (Ogino et al., 2022), equivalent to those above Africa and the Atlantic. A new maximum,
586 equivalent to that found above Africa, is now detected over India, mostly related to human
587 activities (fossil fuel combustion and agriculture burning) (Singh et al., 2020).
588   However, the accurate quantification of TTCO remains a challenge. The following
589 section quantifies the differences between the satellite and in situ data in order to improve the
590 accuracy of TTCO estimates from space.
591
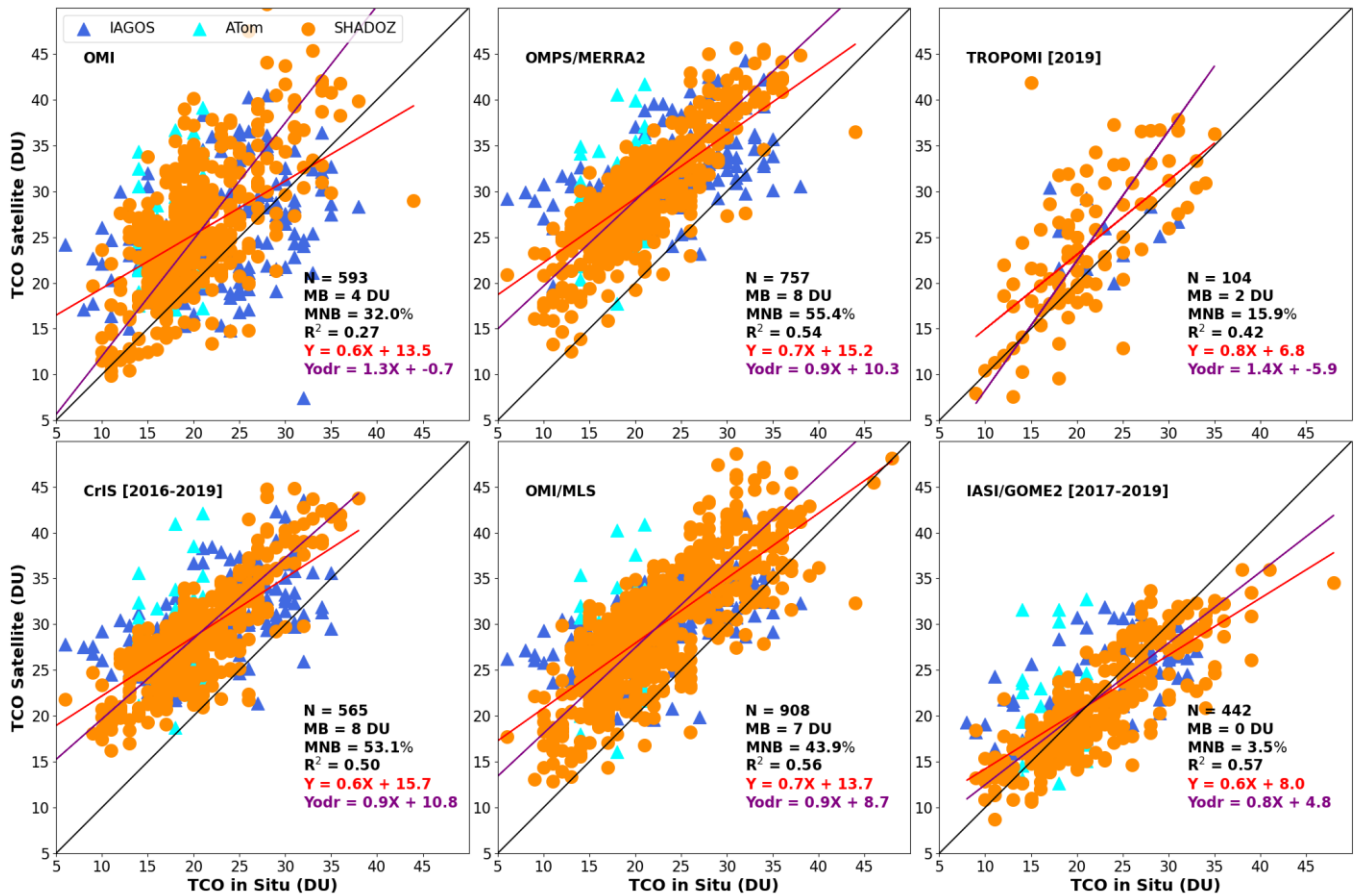592 **3.3 How do the current tropospheric ozone satellite records perform?**
593
594
595
596
597
598

Individual monthly TCO from Satellite versus TCO from IAGOS, SHADOZ and ATom - Nprof/month > 0

599

600

Figure 4. Scatter plot of the monthly TTCO from OMI, OMPS/MERRA2, TROPOMI, CrIS,
OMI/MLS and IASI/GOME2 satellite records compared with the in situ TTCO from IAGOS
(dark blue triangles), ATom (cyan triangles) and SHADOZ (orange circles) between 2014 and
2019. The in situ TTCO values are calculated between the surface and 270 hPa. The TTCO for
all satellite data extends much higher (typically up to 100-150 hPa), except for TROPOMI
(TTCO calculated from the surface up to 270 hPa) and IASI/GOME2 (TTCO up to 12 km/200
hPa) (Figure S1). The linear least-squares regression is shown in red. The linear orthogonal
distance regression is indicated in purple. The number of points (N), the mean biases (MB), the
mean normalized biases (MNB) and the correlation coefficient (R^2) are shown in black. N
corresponds to the number of months with both in situ and satellite data multiplied by the
number of IAGOS regions, ATom regions and SHADOZ sites over the time period 2014-2019.

612

The overall satellite biases of TTCO against in situ TTCO from IAGOS, ATom and
SHADOZ are shown in Figure 4. All satellite TTCO values show an expected positive offset
since the top level of the satellite TTCO lies higher than that of the in situ data, except for
TROPOMI and IASI/GOME2. The mean differences vary from 0 DU to 9 DU. Figure 4 shows a
mean TTCO bias of 2 DU for TROPOMI and no TTCO bias for IASI/GOME2. For TROPOMI

19

618 and IASI/GOME2, showing the lowest TTCO biases, the sign of the differences can change with
619 location (Figure S18). TROPOMI shows positive TTCO biases of 1-4 DU from the Pacific to
620 Africa and negative biases of 1-2 DU above India, Indonesia/Malaysia. IASI/GOME2 also shows
621 negative TTCO biases of 1-5 DU above India and Indonesia/Malaysia. When using only
622 SHADOZ data, rather than all three in situ data sets, as a reference for the TTCO from the
623 surface to 270 hPa (Figure S19), the mean biases remain the same (compared to Figure 4),
624 whereas the correlation coefficient and the mean normalized biases increase.
625

626
627
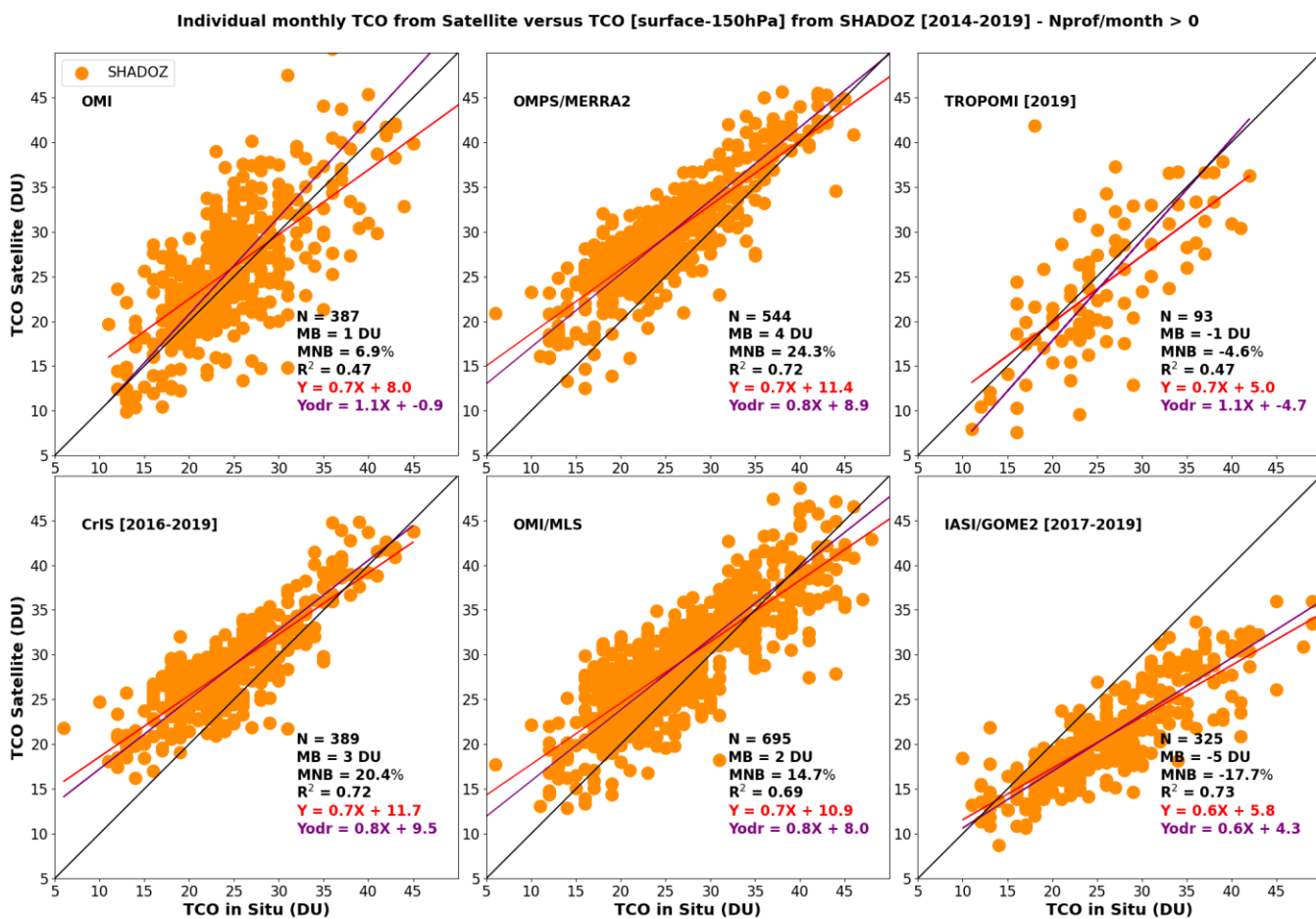
Figure 5. Same as Figure 4 but for satellite data compared with SHADOZ TTCO integrated
629 between the surface and 150 hPa.

630

631   Because four satellite records (OMI, OMPS/MERRA2, CrIS and OMI/MLS) show
632 TTCO from the surface to 100-150 hPa, altitudes that the IAGOS aircraft do not reach, we
633 compare them to SHADOZ TTCO from the surface to 150 hPa (Figure 5). Both the biases and
634 the correlation coefficients improve when compared to results for TTCO up to 270 hPa, except
635 for IASI/GOME2 for which the bias became negative (-5 DU). These results illustrate that
636 differences in the definition of the top level of the tropospheric column play an important role in

637 observed differences between satellite TTCO and in-situ TTCO ozone data. There is hence a
638 need for a common tropospheric column definition to make satellite TTCO estimates comparable
639 between each other and with in-situ data.
640   Looking at the SHADOZ sites individually (Figure S20), the biases became closer to zero
641 above Ascension Island (tropical Atlantic) and Natal (Brazil) when the top level of the column
642 was changed from 270 hPa to 150 hPa. However, the satellite TTCO records with the top level of
643 the column higher than 270 hPa (all satellites except TROPOMI and IASI/GOME2) still
644 overestimate TTCO after changing the reference SHADOZ TTCO's top level from 270 hPa to
645 150 hPa.
646   The biases of TROPOMI reported in Figures 4, S11 and 5 are in the range of those
647 reported in Hubert et al. (2021) with a bias of 2.3±1.9 DU when compared with the SHADOZ
648 ozonesondes. Biases estimated for TROPOMI and IASI/GOME 2 using the three in situ TTCO
649 data sets from the surface to 270 hPa (Figure 4), and biases estimated for OMI,
650 OMPS/MERRA2, CrIS and OMI/MLS using SHADOZ TTCO from the surface to 150 hPa
651 (Figure 5) are applied to improve the accuracy of estimates of the tropospheric ozone burden
652 (TOB), as described in section 3.5.
653
654 **3.4 Ozone changes with time**
655

656
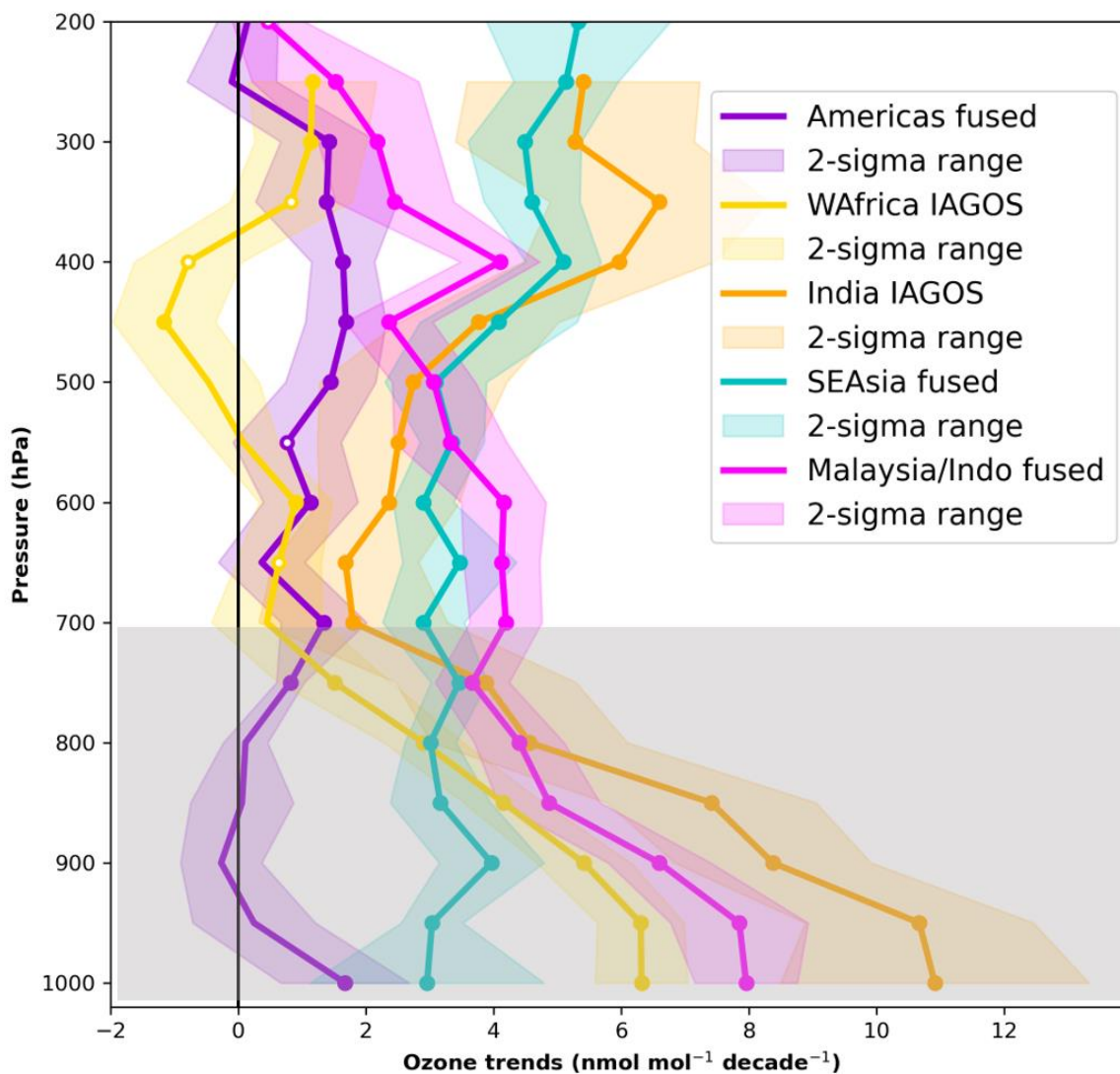
Figure 6. Vertical profiles of ozone trends (nmol mol^{-1} decade^{-1}) between 1994 and 2019, at 50 hPa vertical resolution. Trends are calculated for the 5 IAGOS regions in the tropics: Americas, Western Africa, India, Southeast Asia and Malaysia/Indonesia. SHADOZ data are available for 3 out of the 5 IAGOS regions and used to produce fused trends (IAGOS + SHADOZ). Filled circles indicate trends with *p*-values less than 0.05. Open circles indicate trends with *p*-values between 0.05 and 0.1. The zero-trend value is indicated with a vertical black line. The vertical range below 700 hPa is shaded grey to indicate that the fused trends are based on several sites and airports influenced by different local air masses. The 2-sigma values associated with the ozone trends are shown in shaded colors.

667

668   The estimation of trends of tropospheric ozone in the tropics based on in situ observations
669   is a difficult task as the data are sparse in time and space, as discussed below. In this study, the
670   Americas, Africa, Southeast Asia and Malaysia/Indonesia are regions sampled both by IAGOS
671   and SHADOZ allowing us to improve the trends estimate in the free troposphere (above 700
672   hPa) by fusing both datasets to achieve a greater sample size and a better representation of
673   regional ozone variability (sections 2.5, S1, Figures S2-S3 and Figures S12-S14). Figure 6 shows
674   trends from the fused datasets. We observed increasing ozone levels between 1994 and 2019
675   over Americas (trends ranging from -0.3 ± 0.6 to 1.8 ± 0.7 nmol mol^{-1} decade^{-1} with the vertical
676   levels), Africa (from -0.3 ± 0.6 to 7.4 ± 0.4 nmol mol^{-1} decade^{-1}), India (from 0.9 ± 1.4 to $11 \pm$
677   2.4 nmol mol^{-1} decade^{-1}), Southeast Asia (from 2.5 ± 0.4 to 5.1 ± 0.8 nmol mol^{-1} decade^{-1}) and
678   Malaysia/Indonesia (from 0.5 ± 0.6 to 8.0 ± 0.8 nmol mol^{-1} decade^{-1}). In the boundary layer
679   (<700 hPa), local air masses sampled above SHADOZ sites and IAGOS airports are likely very
680   different in terms of emissions, photochemistry and airmass history, which may explain higher
681   differences between the fused and IAGOS trends than in the free troposphere (Figure S21). The
682   strongest trend we find is 12.5 ± 2.2 nmol mol^{-1} decade^{-1} in the boundary layer over
683   Malaysia/Indonesia using IAGOS data only (Figure S21). Malaysia/Indonesia is the region for
684   which the number of years with missing IAGOS data is excessive (Figure S14). As shown by
685   Gaudel at al. (2020), the "L" shape of the trends, with a rather constant trend above the 700 hPa
686   level and larger trends in the boundary layer, is common to the studied tropical regions except
687   for Southeast Asia, which shows similar trends in both the boundary layer and in the free
688   troposphere. Taking the fused trends as the reference, we find that the trends estimated using
689   IAGOS data only tend to be overestimated by 1-2 nmol mol^{-1} decade^{-1} at 700-500 hPa, except
690   over the Americas, and underestimated by 0.5-1 nmol mol^{-1} decade^{-1} at 500-250 hPa, except over
691   Malaysia/Indonesia. Only IAGOS ozone profiles are available over India and the trends in this
692   region can reach up to 6.7 ± 1.8 nmol mol^{-1} decade^{-1} at 350 hPa, which exceed the trends over the
693   other regions at the same vertical level.
694
695
696
697

Decadal ozone trends for 2004-2019, based on the annual ozone anomaly relative to 2004-2019
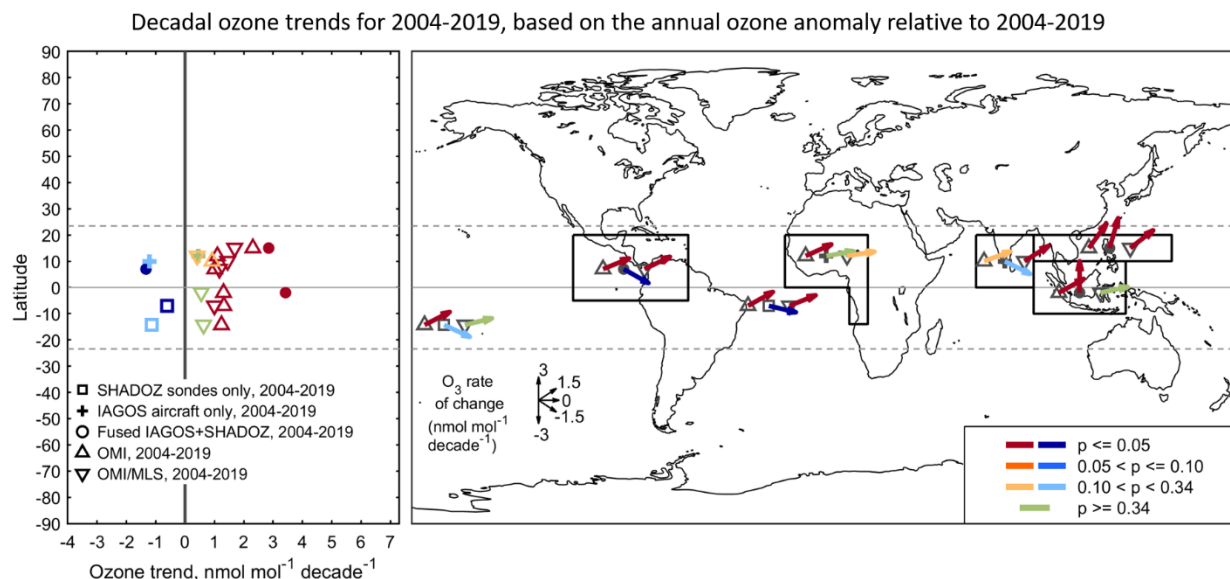
Figure 7. TTCO trends (nmol mol^{-1} decade^{-1}) between 2004 and 2019 from IAGOS (crosses), SHADOZ (squares), IAGOS fused with SHADOZ (circles), OMI (triangles up) and OMI/MLS (triangles down) above the five continental IAGOS regions (Americas, Africa, India, Southeast Asia and Malaysia/Indonesia) and two oceanic SHADOZ regions (Samoa and Natal + Ascension Island). The left panel shows the trends of ozone as a function of latitude. The right panel shows the trends of ozone on the map with the black rectangles demarcating the five IAGOS regions. On the map, the longitude of the crosses, circles, triangles and squares are arbitrary and the latitude is the mean latitude of the black rectangles or relative to the SHADOZ sites. The direction of the arrows shows the magnitude of the trends and the colors indicate the *p*-value. The TTCO trends from in situ data are calculated from the monthly TTCO between the surface and 100 hPa, except over India where IAGOS profiles are available between the surface and around 200 hPa. The TTCO trends from OMI and OMI/MLS are calculated from the monthly TTCO defined between the surface and around 102-105 hPa (Figure S1).

Satellite data from OMI are available continuously since 2004 and 15-year trends can now be estimated. The interannual variability of the TTCO from satellite and in situ data is shown in Figure S22. Several time series of the monthly mean of tropospheric ozone above Malaysia/Indonesia show the influence of climate variability such as El Niño and related fires. For example, we see a peak of ozone in September 2015 in agreement with a peak of CO emissions due to biomass burning above Equatorial Asia (Figure S23, Mead et al., 2018).
Figure 7 and Table 1 show the trend estimates of TTCO in nmol mol^{-1} decade^{-1} from OMI CCD, OMI/MLS, and in situ data between 2004 and 2019. The in situ trends between 2004 and 2019 (Figure S24 and Table 1) are negative for Samoa (-1.1 ± 1.9 nmol mol^{-1} decade^{-1}), Americas (-1.3 ± 0.4 nmol mol^{-1} decade^{-1}), Natal/Ascension Island (-0.6 ± 0.5 nmol mol^{-1} decade^{-1}) and India (-1.2 ± 1.8 nmol mol^{-1} decade^{-1}), and positive for Western Africa (0.4 ± 1 nmol mol^{-1} decade^{-1}), Southeast Asia (2.9 ± 1.4 nmol mol^{-1} decade^{-1}) and Malaysia/Indonesia

24

726   $(3.4 \pm 1.3$ nmol mol^{-1} decade^{-1}). The presence of negative trends above some regions for the
727   shorter 2004-2019 period differs greatly from the longer 1994-2019 time period which had no
728   time series with negative trends except above Samoa (Figure 7, Table 1). They also differ from
729   the positive trends shown by the satellite data (full record, Figure 7, Table 1). The satellite trends
730   vary between 0.9 ± 1.3 nmol mol^{-1} decade^{-1} over India and 2.3 ± 1.3 nmol mol^{-1} decade^{-1} over
731   Southeast Asia with OMI, and between 0.4 ± 0.8 nmol mol^{-1} decade^{-1} over Western Africa and
732   1.7 ± 0.8 nmol mol^{-1} decade^{-1} over Southeast Asia with OMI/MLS (Figure 7, Table 1).
733   Discrepancies between satellites and in situ observations in assessing trends may be
734   caused by (i) the different definitions of the tropospheric column (100 hPa, 200 hPa or
735   tropopause defined with the temperature lapse rate); (ii) the diminished sensitivity of the space-
736   based instruments in the boundary layer; or (iii) the limited data availability and relatively short
737   record that may lead to less accurate and precise trends (Figures S2 and S3). In particular we
738   highlight previous research that has demonstrated the difficulty in detecting ozone trends in time
739   series that are noisy and or sparsely sampled (Weatherhead et al., 1998; Fischer et al., 2011;
740   Barnes and Fiore, 2016; Fiore et al., 2022). These studies show that 20 years of observations, or
741   more, are needed for trend detection, and that model ensembles (based on differing initial
742   conditions) can produce trends for a given location that vary so widely that even the sign can
743   fluctuate between positive and negative, when dealing with time periods less than 20 years.
744   Furthermore, previous studies of in situ ozone profiles concluded that a sampling frequency of
745   once per week generally fails to produce accurate monthly mean and trend values (Logan, 1999;
746   Saunois et al., 2012; Chang et al., 2020, 2022). Consistent with these previous studies, we
747   conducted our own analysis of tropical ozone time series (see the Supplementary Section S1) and
748   found that these sparsely sampled data sets have very low signal-to-noise ratios, which makes
749   trend detection very difficult, especially when a time series is less than 20 years in length (Chang
750   et al., 2020,2022). The comparison between the in situ and satellite trends is only 15 years in
751   length (2004-2019), and the in situ datasets are sparsely sampled, characteristics consistent with
752   known challenges for trend detection. Furthermore, we point out that the robustness of the
753   positive trends from the satellite records greatly diminishes, and even becomes undetectable,
754   when we reduce the sample size of the satellite data in the IAGOS regions to match the sparse
755   sampling frequency of the aircraft observations (Figure S25). For example, when the satellite
756   data are fully sampled across the five IAGOS domains, all trends are positive, within the range
757   0.4 ± 0.8 to 2.3 ± 1.3 nmol mol^{-1} decade^{-1}. But when the satellite sample sizes are reduced so
758   that they only coincide with the specific months and grid-cells sampled by the IAGOS aircraft,
759   the range of the trends more than doubles and even includes negative values (-3.1 ± 2.6 to $+3.6 \pm$
760   2.1 nmol mol^{-1} decade^{-1}). This increased uncertainty is an expected outcome of decreased
761   sampling frequency, as illustrated in Figure S2.
762   The color scheme in Table 1 reflects our overall confidence in the presence of in situ
763   trend estimates, according to the number of missing monthly values, monthly average data
764   availability, the length of study period, and the p-value of the trend estimate (the trends are
765   confident only if a low p-value and a high data coverage are met, see Appendix A for further
766   details and Section S3 for a discussion of the confidence assigned to each region). When
767   assigning a level of confidence to a trend we weigh the p-value and the data coverage and ask the
768   question: "Are we confident that a positive or negative trend is reliable?" For example, if a
769   positive trend has a low p-value but also low data coverage then our confidence that the trend is
770   reliable is diminished. Western Africa is the only region in this study with sufficient sampling
771   for reliable trend detection with high confidence (1994-2019). Trends derived from the other in

772 situ time series only have low or medium confidence due to sampling deficiencies and/or low
773 estimation certainty (based on the p-value). When we compare the satellite trends to the in situ
774 trends we find that they are consistent for Southeast Asia, with all three data sets showing
775 positive trends. In the other regions we find discrepancies between the in situ and satellite trends,
776 but in these regions, we do not have high confidence in the in situ trends, and therefore there is
777 no reason to reject the satellite trend values, which generally indicate an increase of ozone in the
778 study regions. However, the discrepancies between satellite and in situ trends in the Americas
779 and Natal + Ascension Island are nuanced and require further discussion. In the Americas region
780 we assigned medium confidence to the decreasing ozone trends based on the in situ observations,
781 which contrasts strongly with the clear positive trends based on the satellite data. When we
782 reduced the satellite sampling coverage to match the locations and months with IAGOS
783 observations, we found that the satellite trends switched from clear positive trends to clear
784 negative trends (Figure S25). This exercise indicates that the available in situ observations are
785 not representative of the large region, and therefore they do not provide sufficient justification
786 for rejecting the positive trends reported by the satellite data. In situ ozone trends above Natal +
787 Ascension Island have a weak negative trend (-0.62 ± 0.54 nmol mol^{-1} decade^{-1}) with medium
788 confidence, while the satellite trends show weak positive trends. While the divergence between
789 the positive and negative trends is small over this short time period (2-3 nmol mol-1 over 15
790 years), this discrepancy warrants further investigation to determine the differences between the
791 satellite and in situ time series trends.
792
793 **3.5 Comparison to previous studies**
794 　　　Using the ozonesondes from the SHADOZ network, Thompson et al. (2021) found
795 positive annual trends of about 1.2 ± 3 % decade^{-1} to 1.9 ± 3 % decade^{-1} (0.08 ± 1.68 nmol mol^{-1}
796 decade^{-1} to 0.78 ± 1.66 nmol mol^{-1} decade^{-1}) between 1998 and 2019 at 5-10 km (~500-250 hPa)
797 across the tropical belt. They reported maximum trends (1.9 ± 3 % decade^{-1}) above the
798 Malaysia/Indonesia (Kuala Lumpur + Java) and Americas (San Cristobal + Paramaribo) regions
799 and minimum trends (1.2 ± 3 % decade^{-1}) above Africa (Nairobi). The SHADOZ trends are
800 slightly lower than the IAGOS + SHADOZ fused trends or IAGOS trends which may be
801 explained by the different starting points of the time series (1998 for SHADOZ data and 1994 for
802 IAGOS data), but they are all positive.
803 　　　Previous studies of TTCO trends from satellite data relied on data harmonization in order
804 to combine several satellite records into a time series spanning at least two decades and to better
805 account for the climate variability in the trend estimates (Heue et al., 2016; Leventidou et al.,
806 2018; Ziemke et al., 2019; Pope et al., 2023). Heue et al. (2016) found a tropical trend of $0.7 \pm$
807 0.12 DU decade^{-1}, with regional trends ranging from $+1.8$ DU decade^{-1} on the African Atlantic
808 coast, to -0.8 DU decade^{-1} over the western Pacific Ocean. Leventidou et al. (2018) reported
809 positive trends of TTCO of 1 to 1.5 DU decade^{-1} between 1996 and 2015 over Northern South
810 America, North Africa, South Africa and India, and negative trends of -1.2 to -1.9 DU decade^{-1}
811 above the oceans (Pacific, Atlantic, Indian oceans). Using TOMS-OMI/MLS, Ziemke et al.
812 (2019) reported positive trends between 1979 and 2016 across the tropical latitude band 20˚S-
813 20˚N except above the southeastern tropical Pacific Ocean and southeastern Indian Ocean. The
814 highest positive trends (up to 1.3 DU decade^{-1}) were found above South-Southeast Asia and
815 Central Africa. Finally, a new harmonized product that quantifies ozone between the surface and
816 450 hPa reports much higher tropical trends than the other studies, with increases of 2.9 ± 1.6

817 DU decade^{-1} for the southern tropical band (0 – 15º S) and 3.9 ± 1.8 DU decade^{-1} for the northern
818 tropical band (0 – 15º N) for the years 1996-2017 (Pope et al., 2023). While these findings vary
819 regarding the magnitude of trends in the tropics, when taken into consideration with the 1994-
820 2019 in situ trends reported by the present study, the preponderance of evidence indicates a
821 general increase of TTCO since the mid-1990s.
822   Wang et al. (2022) report an increase of TTCO (950 - 250 hPa) trends using the GEOS-
823 Chem chemical transport model above the IAGOS' regions and SHADOZ sites between 1995
824 and 2017, except above Samoa. The trends vary with locations between -0.60 ± 0.38 nmol mol^{-1}
825 decade^{-1} above Samoa and 2.87 ± 0.23 nmol mol^{-1} decade^{-1}. In general, they find that the TTCO
826 trends from the model are lower by 1-3 nmol mol^{-1} decade^{-1} than from the observations, except
827 above Paramaribo.
828
829

Table 1. Summary of the TTCO trends in nmol mol^{-1} decade^{-1} from IAGOS, SHADOZ, OMI/MLS and OMI CCD.

The sampling column reports three numbers for the in situ data: i) the number on the top refers to the average number of profiles per months taking into account all the months with profiles, ii) the number in the middle refers to the percentage of months with data for the studied time-period (1994-2019 or 2004-2019), iii) the number in the bottom refers to the total number of profiles for the studied time period (1994-2019 or 2004-2019). For the satellites, the sampling column reports "Full" when the full record is taken into account and "Filtered" when the satellite sample sizes have been greatly reduced so that they only coincide with the specific months and grid-cells sampled by the IAGOS aircraft. The table cells are color coded to reflect the low confidence (light blue), medium confidence (blue) and high confidence (dark blue) on the ozone trends from the in situ data based on the sampling and the p-value.

		1994-2019			2004-2019		
		Trends±2σ (nmol mol^{-1} decade^{-1})	p-value	Sampling	Trends±2σ (nmol mol^{-1} decade^{-1})	p-value	Sampling
IAGOS	Western Africa	2.34±0.48	<0.01	18.8 71.8% 3411	0.44±1.04	0.40	20.2 66.7% 2261
	India	5.68±1.06	<0.01	7.6 66.7% 1574	-1.21±1.76	0.17	8.5 67.7% 1100
SHADOZ	Samoa	-0.03±1.21	0.97	3.2 92.8% 779	-1.13±1.90	0.23	3.1 91.6% 537
	Natal + Ascension Island	0.49±0.49	0.04	6.3 90.4% 1426	-0.62±0.54	0.01	6.0 87.2% 939
Fused IAGOS + SHADOZ	Americas	0.47±0.79	0.36	12.2 92.2% 3642	-1.33±0.39	<0.01	10.7 93.6% 2036
	Southeast Asia	3.51±0.78	<0.01	11.2 77.8% 2501	2.85±1.38	<0.01	10.2 82.8% 1730
	Malaysia/Indonesia	3.96±0.53	<0.01	5.0 89.8% 1445	3.42±1.35	<0.01	4.7 89.9% 954
OMI CCD	Americas				1.01±0.72	0.01	Full
					-3.06±2.65	0.02	Filtered
	Western Africa				1.10±1.04	0.04	Full
					-1.04±3.08	0.50	Filtered
	India				0.92±1.26	0.15	Full
					1.20±2.95	0.42	Filtered
	Southeast Asia				2.31±1.34	<0.01	Full
					3.56±2.08	<0.01	Filtered
	Malaysia/Indonesia				1.31±1.15	0.02	Full
					2.26±3.42	0.19	Filtered
	Samoa				1.24±1.17	0.04	
	Natal + Ascension Island				1.32±1.04	0.01	
OMI/MLS	Americas				1.17±0.72	<0.01	Full

				-2.79±1.96	0.01	Filtered
	Western Africa				0.41±0.80	0.30	Full
				0.68±3.95	0.73	Filtered
	India				1.45±0.79	<0.01	Full
				-1.64±1.67	0.05	Filtered
	Southeast Asia				1.69±0.83	<0.01	Full
				2.46±1.85	0.01	Filtered
	Malaysia/Indonesia				0.55±1.22	0.37	Full
				1.39±4.36	0.53	Filtered
	Samoa				0.63±1.34	0.35	
	Natal + Ascension Island				1.00±0.78	0.01	

842

843

844

845

846 **3.6 Tropospheric ozone burden**

847

848

849
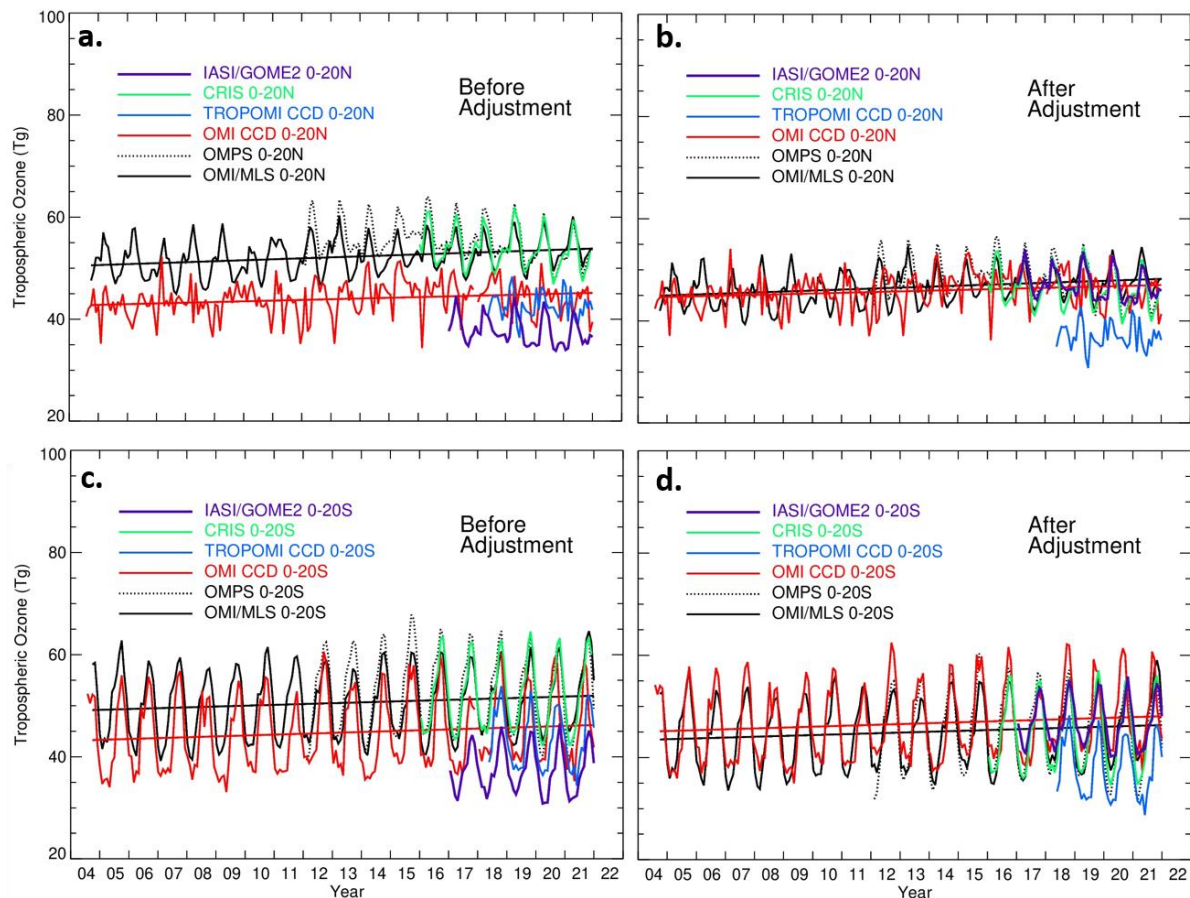
850

851 <mark>**Figure 8.** Time series of tropospheric ozone burden (Tg) from OMI/MLS, OMPS/MERR2, OMI</mark>

852 <mark>CCD, TROPOMI, CrIS and IASI/GOME2. The panels show the monthly means for the Northern</mark>

853 <mark>Hemisphere (a and b) and the Southern Hemisphere (c and d) before and after bias correction.</mark>

854 <mark>The biases we used are in DU and from the differences between IASI/GOME2 and TROPOMI</mark>

855 <mark>TTCO using the reference TTCO up to 270 hPa and between OMI, OMI/MLS,</mark>

856 <mark>OMPS/MERRA2, CrIS TTCO using the reference TTCO up to 150 hPa (Figures 4 and 5).</mark>

857

858

859   Figure 8 shows the time series of the tropical tropospheric ozone burden (TTOB, Tg)

860 from six satellite records. As described in the Methods, OMI/MLS, OMI CCD,

861 OMPS/MERRA2, TROPOMI, CrIS, and IASI/GOME2 are sampled in the 20˚S-20˚N latitude

862 band. For both hemispheres we find two distinguished groups in terms of TTOB (Figure 8,

863 panels a and c<mark>): (i) TROPOMI and IASI/GOME2 with a range of TTOB of 35-45 Tg, (ii)</mark>

864 <mark>OMI/MLS, OMPS/MERRA2 and CrIS with a range of TTOB of 40-65 Tg. These differences are</mark>

865 <mark>explained by the difference of the upper bound of the tropospheric column (lower for TROPOMI</mark>

866 <mark>and IASI/GOME2 than for the other satellite data). OMI CCD TTOB (35-55 Tg) falls between</mark>

867 these two groups. The seasonal variability of TTOB is lower in the northern hemisphere than in
868 the southern hemisphere.
869   The biases calculated from the scatter plots of satellite versus ozonesondes (Figures 4 and
870 5) are used to correct the satellite time series. The adjustment reduced the differences by about
871 10 Tg in the northern hemisphere and by 5 Tg in the southern hemisphere, between the two
872 groups mentioned above. After adjustment, OMI CCD TTOB become close to (northern
873 hemisphere) or higher than (southern hemisphere) OMI/MLS TTOB. In the northern hemisphere,
874 after adjustment (Figure 8, panels b and d, and Table 2), TROPOMI TTOB (30-40 Tg) are lower
875 than for the other datasets (40-55 Tg). In the southern hemisphere, it is difficult to distinguish the
876 two groups, after adjustment. TROPOMI TTOB (30-48 Tg) shows lower values than the other
877 datasets (30-60 Tg) but the average differences are smaller than in the northern hemisphere.
878   Table 2 summarizes TTOB trends from this study, and from TOAR-Climate (Gaudel et
879 al., 2018). Trends are positive and higher in the northern hemisphere (1.6 ± 1.1 Tg decade^{-1} to
880 5.7 ± 2.5 Tg decade^{-1}) than the southern hemisphere (0.9 ± 2.2 Tg decade^{-1} to 5.1 ± 4.5 Tg
881 decade^{-1}). Because TTOB trends in Tg decade^{-1} can increase with the width of the latitude band
882 (assuming trends are all positive across the range of latitudes considered), we also report trends
883 in % decade^{-1}, to compare trends between different latitude bands. The 2004-2016 OMI/MLS
884 trends in the 0-30° north and south latitude bands are higher by a factor of 3 or 5 than the 2004-
885 2019 OMI/MLS trends in the 0-20° north and south latitude bands. These differences might be
886 explained by the influence of the larger increases of subtropical tropospheric ozone.
887
888

889 **Table 2**. Summary of tropical tropospheric ozone burden values and trends.

890

	Latitude band	Tropospheric Ozone Burden			Trends			
		Period	Instrument/ model	Values Tg	Period	Instrument	Values Tg/decade	Values %/decade
This study (These numbers are corrected using bias results from Figure 5)	0-20˚N	2004-2021	OMI/MLS	**46.6** ± 7.0	2004-2019	OMI/MLS	**1.6** ± 1.1	**3** ± 2
		2004-2021	OMI	**45.9** ± 6.8	2004-2019	OMI	**2.4** ± 1.1	**5** ± 2
		2012-2021	OMPS	**48.1** ± 7.4				
		2016-2021	CrIS	**46.4** ± 7.5				
		2017-2021	IASI/GOME2	**38.1** ± 5.9				
		2019	TROPOMI	**34.9** ± 5.1				
	0-20˚S	2004-2021	OMI/MLS	**44.9** ± 13.0	2004-2019	OMI/MLS	**0.9** ± 2.2	**2** ± 5
		2004-2021	OMI	**46.5** ± 14.2	2004-2019	OMI	**1.9** ± 2.4	**4** ± 5
		2012-2021	OMPS	**45.3** ± 15.1				
		2016-2021	CrIS	**44.6** ± 13.4				
		2017-2021	IASI/GOME2	**37.1** ± 8.6				
		2019	TROPOMI	**34.7** ± 10.7				
TOAR-Climate (Figures S28, S29)	0-30˚N				2004-2016	OMI/MLS	**5.7** ± 2.5	**7** ± 3
	0-30˚S				2004-2016	OMI/MLS	**5.1** ± 4.5	**6** ± 5.6

891

892

893

4. Conclusions

Long and mid-term records of tropospheric ozone from IAGOS, SHADOZ, and OMI, as well as new observations from the ATom aircraft campaign and the CrIS, IASI/GOME2 satellite instruments are now available in the tropics, a region undergoing rapid changes in terms of human activity and emissions of ozone precursors. The present study takes advantage of these new data records to assess the distribution of tropical tropospheric ozone, and it uses the longest records to assess its trends:

Present-day distribution

- With greater availability of ozone profiles across the tropics we can now demonstrate that southern India is among the most polluted regions (Western Africa, tropical South Atlantic, Southeast Asia, Malaysia/Indonesia) with 95th percentile ozone values reaching 80 nmol mol^{-1} in the lower free troposphere, comparable to mid-latitude regions, such as Northeast China/Korea. – Section 3.1, Figure 2
- The lowest ozone values (5th percentile) are less than 10 nmol mol^{-1}, and are observed by SHADOZ and ATom in the boundary layer (below 700 hPa) above the Americas and the tropical South Pacific. – Section 3.1, Figure 2
- From space, the distribution of tropical tropospheric column ozone (TTCO) ranges from 10 to 40 DU in the 20°S-20°N latitude band – Section 3.2, Figure 3
- The definition of the tropospheric column plays an important role in assessing tropical tropospheric ozone. Satellite data with a higher upper limit overestimate tropical column ozone compared to in-situ data. Mean biases reach up to 9 DU for OMPS/MERRA2 when compared to IAGOS, ATom and SHADOZ. The bias is 0 for IASI/GOME2 for which the column definition matches the in situ observations. – Section 3.3, Figure 4
- The smallest biases (≤ 2 DU) are found when matching the top limit of the in situ profiles to that of the OMI, TROPOMI and IASI/GOME2 satellite records. – Section 3.3, Figures 4 and 5
- The in situ observations were critical for adjusting the biases in the satellite products, bringing them into closer alignment. In the 20˚S-20˚N latitude band, the tropical tropospheric ozone burden (TTOB) is slightly larger in the northern hemisphere (between 34.9 ± 5.1 and 48.1 ± 7.4 Tg) than in the southern hemisphere (between 34.7 ± 10.7 and 46.5 ± 14.2 Tg). The seasonal variability of TTOB is in the northern hemisphere than in the southern hemisphere. – Section 3.6, Figure 8 and Table 2

Trends

- When focusing on the longest available records exceeding 20 years (1994-2019, IAGOS/SHADOZ data reported in this study) or 30 years (1979-2016 satellite record reported by Ziemke et al., 2019) we see a consistent picture of increasing ozone across the tropics. IAGOS and SHADOZ data were fused to increase the sample sizes and to improve the statistics of the data over three out of the five IAGOS regions: Americas, Southeast Asia, Malaysia/Indonesia (Western Africa and India with no SHADOZ data). India and Malaysia/Indonesia are the regions with the strongest ozone increase below 800 hPa (11 ± 2.4 and 8 ± 0.8 nmol mol^{-1} decade^{-1} close to the surface, respectively) and India above 400 hPa (up to 6.8 ± 1.8 nmol mol^{-1} decade^{-1}). Southeast Asia and Malaysia/Indonesia show the highest increase in the mid-troposphere (550-750 hPa, up to

33

3.4 ± 0.8 and 4 ± 0.5 nmol mol^{-1} decade^{-1}, respectively). Trends of the tropical tropospheric column ozone reflect these results. In terms of in situ trend reliability based on data availability and *p*-value of trend estimate, we have the most confidence in Western Africa (while it is still not ideal due to moderate data gaps) and the least confidence in Samoa and Americas. – Section 3.4, Figure 6

- For shorter time periods (< 20 years) trend detection can be even more challenging due to the larger additional uncertainty associated with sparsely sampled ozone records. – Section 3.4, Figure 7 and S24

- The OMI and OMI/MLS satellite records have a very high sampling frequency compared to the sparse in situ datasets and mostly show positive 15-year (2004-2019) trends above the IAGOS regions (from 0.55 ± 1.22 to 2.31 ± 1.34 nmol mol^{-1} decade^{-1}) with the maximum trends over Southeast Asia of 2.31 ± 1.34 nmol mol^{-1} decade^{-1} with OMI CCD, and 1.69 ± 0.89 nmol mol^{-1} decade^{-1} with OMI/MLS. The strongest agreement between satellite and in situ trends is found above Southeast Asia where TTCO had increased at a rate of about 2-3 nmol mol^{-1} decade^{-1}. These trends are consistent with the results from Ziemke et al. (2019) using TOMS-OMI/MLS records and Gaudel et al. (2020) using IAGOS ozone profiles. Above the other regions, we only have low to medium confidence in the in situ trends, therefore we concluded that we have no reason to reject the positive tropical tropospheric ozone trends based on satellite data. However, the discrepancy between the weak positive satellite trends and the weak negative in situ trends above Natal + Ascension Island warrants further investigation. – Section 3.4 and 3.5, Figure 7 and Table 1

This study demonstrates that most tropical regions require either an increased and/or continuous sampling (in situ and remote sensing) of ozone because either there are no data, or the data are so sparse that it is difficult to estimate accurate and precise trends to evaluate the satellite records. However, we also demonstrate that the current sampling frequency is adequate for bias correcting the satellite products, as shown in Figure 8.

TROPOMI, IASI/GOME2, CrIS and OMPS/MERRA2 are recently available satellite records and their overlap for several years with the OMI record will assure continuity of ozone and precursors observations from space when the NASA Aura mission terminates by 2025. GEMS, the only geostationary mission covering the tropics (tropical Asia), will bring new capabilities in monitoring the region with the strongest ozone increases in the world, with higher spatial and temporal resolution than the polar orbiting instruments. This study underscores the importance of harmonizing TTCO data records such that they have a common vertical top level of the tropospheric column. Additionally, there is a pressing need for common profile retrieval schemes for different nadir sensors, such as those provided by initiatives like TROPESS (TRopospheric Ozone and its Precursors from Earth System Sounding, https://tes.jpl.nasa.gov/tropess/).

Moreover, to better understand the drivers behind the observed increases in TTOB, it is essential to conduct simulations using global chemical transport models, chemistry climate models, Earth system models, and regional models spanning recent decades.

979   Encouragingly, these endeavors have been newly proposed within the framework of the
980 Tropospheric Ozone Assessment Report phase II (TOAR-II), an initiative under the International
981 Global Atmospheric Chemistry (IGAC) project. These efforts will be the focus of forthcoming
982 publications featured in the TOAR-II Community Special Issue.
983   It is also worth noting that the TOAR-II Community Special Issue will include similar
984 trends analysis applied at global scale using IAGOS, Ozonesondes, FTIR, and Brewer/Dobson
985 (Umkehr) data.
986
987

Appendix A

The Intergovernmental Panel on Climate Change (IPCC) developed a guidance note for the consistent treatment of uncertainties (Mastrandrea et al., 2010) that was followed by the fifth and sixth IPCC assessment reports. Among other applications, the calibrated language described by the guidance note is helpful for the discussion of long-term trends and for communicating the level of confidence that an author team wishes to assign to a particular trend value, or to an ensemble of trend values. Confidence in the validity of a finding is expressed qualitatively with five qualifiers (very low, low, medium, high and very high), based on the type, amount, quality, and consistency of the available evidence, and the level of agreement among studies addressing the same phenomenon (see Figure 1 of Mastrandrea et al., 2010).

Following IPCC, the Tropospheric Ozone Assessment Report (TOAR) developed its own guidance note on best statistical practices for TOAR analyses, featuring an uncertainty scale for assessing the reliability and likelihood of the estimated trend (Chang et al., 2023). The uncertainty scale has five qualifiers as follows: very low certainty or no evidence, low certainty, medium certainty, high certainty and very high certainty. Each qualifier corresponds to a range of values associated with either the signal-to-noise ratio or the p-value of the trend. A limitation of the uncertainty scale is that it is best suited for surface ozone time series with high frequency sampling, which allows for robust calculation of monthly means, upon which the trends are calculated. For the case of calculating trends based on sparse ozone profiles, in many cases the monthly means are biased or unreliable due to low sampling frequency, which adds additional uncertainty to the calculation of the trend. Because the p-value (or the signal-to-noise ratio) of a trend based on monthly means does not consider the impact of low sampling frequency on the monthly means, we developed new calibrated language to express our confidence in trends based on sparse ozone profiles.

Following the methodology of IPCC (Mastrandrea et al., 2010) Table A1 presents a confidence scale that we use in this present study to express our confidence in a trend based on sparse ozone profiles (as reported in Table 1 in the main text). Any line fit though a time series will produce a trend value that is either positive or negative, and we use this scale to answer the question: "Are we confident that a positive or negative trend is reliable?". The confidence scale considers both data coverage (based on the number of profiles per month and continuity of sampling) and the estimation of the uncertainty of the trend, based on the p-value and the 95% confidence interval. Higher confidence can be placed on trends with lower p-values and greater data coverage, while less confidence is placed on trends with relatively high p-values and low data coverage. The selection of a particular confidence level is qualitative, with no sharp boundaries, however the following guidelines inform our decision-making:

Data coverage: Previous studies (Logan, 1999; Saunois et al. 2012; Chang et al., 2020) have shown that sampling rates of once per week (or less) fail to provide accurate monthly means, while increased sampling rates of 2 or 3 times per week are more accurate. The most accurate sampling rate is 4 times per week or higher. Continuous data records with no, or limited gaps, are more reliable than records with multiple or large gaps. Data length also plays a role in trend

1029 reliability. A time series with more than 90% of months with data, and with more than 15
1030 profiles per month is considered to have high data coverage. A time series with 66 to 90% of
1031 months with data, and with 7-15 profiles per month is considered to have moderate data coverage
1032 (this also applies to a region that only meets one condition for high data coverage). A time series
1033 that has less than 66% of months with data, or less than 7 profiles per month has low data
1034 coverage. It should be noted that, based on our criteria, none of the current study regions meet
1035 the criteria for high data coverage, and therefore the top row in Table A1 is not applicable to this
1036 study. In addition, since we derive the trends based on either a 25-year or a 15-year record, it is
1037 natural to consider the trends derived from a longer data record are more robust, as a record
1038 length less than two decades is generally insufficient to eliminate the impact of interannual
1039 variability (Weatherhead et al., 1998; Barnes et al., 2016; Fiore et al., 2022). Therefore, all of the
1040 time series in Table 1 with 15-year records are considered to have low data coverage.

1041 **Estimation uncertainty:** In general, lower *p*-values and higher signal-to-noise ratios are
1042 indicators of a robust trend. The "Guidance note on best statistical practices for TOAR analyses"
1043 (Chang et al., 2023) assigns the following degrees of certainty according to *p*-value: very high
1044 certainty ($p \leq 0.01$), high certainty ($0.05 \geq p > 0.01$), medium certainty ($0.10 \geq p > 0.05$), low
1045 certainty ($0.33 \geq p > 0.10$), very low certainty or no evidence ($p > 0.33$). We acknowledge that
1046 the trends calculation does not consider the inherent quality of the data (i.e. accuracy and
1047 precision of the data), which will be explore in future studies within TOAR Phase II.

1048

1049

1050 **Table A1**. Calibrated language for discussing confidence in long-term trend estimates based on
1051 ozone profiles. Data coverage refers to the number of ozone profiles in a month, and the number
1052 of months with available data. Estimation uncertainty refers to the uncertainty of a trend line
1053 drawn through monthly means, as quantified by the p-value and the 95% confidence interval.

↑ **Data coverage** (based on the number of profiles per month and continuity of sampling)	**medium confidence** low estimation certainty high data coverage	**high confidence** moderate estimation certainty high data coverage	**very high confidence** high estimation certainty high data coverage
	low confidence low estimation certainty moderate data coverage	**medium confidence** moderate estimation certainty moderate data coverage	**high confidence** high estimation certainty moderate data coverage
	very low confidence or no evidence low estimation certainty low data coverage	**low confidence** moderate estimation certainty low data coverage	**medium confidence** high estimation certainty low data coverage
	Estimation uncertainty → (based on p-value)		

1054

1055

1056

1057

1058

Author contributions

Conception and design of the study: AG, IB, ML, K-LC, OC

Generation, collection, assembly, analysis and/or interpretation of data: AG, IB, ML, K-LC, OC

JZ, BS, AMT, RS, DEK, NS, DH, AK, JC, K-PH, PV, KA, JP, CT, TBR

Drafting and/or revision of the manuscript: AG, IB, ML, K-LC, OC, JP, KA, AMT, RS, DH,

AK, NS, JZ, GJF, BCM

All authors approved for submission of the manuscript.

Competing interests

ORC is the Scientific Coordinator of the TOAR-II Community Special Issue, to which this paper

has been submitted, but he is not involved with the anonymous peer-review process of this or

any of the other papers submitted to the Special Issue journals.

Data Availability

The monthly quasi-biennial oscillation values can be found at https://www.geo.fu-berlin.de/met/ag/strat/produkte/qbo/qbo.dat.

The monthly El Niño-Southern Oscillation index can be found at https://psl.noaa.gov/enso/mei/.

ATom data are archived at https://daac.ornl.gov/ATOM/guides/ATom_merge.html and are published through the Distributed Active Archive Center for Biogeochemical Dynamics (Wofsy et al., 2018).

IAGOS ozone profiles can be found at https://iagos.aeris-data.fr/.

SHADOZ ozone profiles can be found at https://tropo.gsfc.nasa.gov/shadoz/ (see reference list).

IASI+GOME2 satellite data can be found at https://iasi.aeris-data.fr/o3_iago2/, last access 08/02/2023.

OMI CCD, OMI/MLS and OMPS/MERRA2 can be found at https://acd-ext.gsfc.nasa.gov/Data_services/cloud_slice/.

TROPOMI CCD can be found at NASA EarthData repository: https://disc.gsfc.nasa.gov/datasets?keywords=tropomi&page=1

CrIS can be found at https://disc.gsfc.nasa.gov/ (see the Method section for more details on the data preprocessing)

The fused datasets and trends (including uncertainty and p-value associated with trend estimate, and fitted coefficients for ENSO/QBO in equation [1] of Section 2.5) can be found at https://csl.noaa.gov/groups/csl4/modeldata/.

References

Archibald, A.T. et al.: Tropospheric Ozone Assessment Report: A critical review of changes in the tropospheric ozone burden and budget from 1850 to 2100. Elementa: Science of the Anthropocene, 8(1), doi:10.1525/elementa.2020.034, 2020.

Barnes, E.A., Fiore, A.M. and Horowitz, L.W.: Detection of trends in surface ozone in the presence of climate variability. Journal of Geophysical Research: Atmospheres, 121(10), pp.6112-6129, 2016.

Blot, R., Nédélec, P., Boulanger, D., Wolff, P., Sauvage, B., Cousin, J.-M., Athier, G., Zahn, A., Obersteiner, F., Scharffe, D., Petetin, H., Bennouna, Y., Clark, H., and Thouret, V.: Internal consistency of the IAGOS ozone and carbon monoxide measurements for the last 25 years, Atmos. Meas. Tech., 14, 3935–3951, https://doi.org/10.5194/amt-14-3935-2021, 2021.

Bourgeois, I., Peischl, J., Thompson, C.R., Aikin, K.C., Campos, T., Clark, H., Commane, R., Daube, B., Diskin, G.W., Elkins, J.W. and Gao, R.S.: Global-scale distribution of ozone in the remote troposphere from the ATom and HIPPO airborne field missions. Atmospheric Chemistry and Physics, 20(17), pp.10611-10635, 2020.

Bourgeois, I., Peischl, J., Thompson, C. R., Aikin, K. C., Campos, T., Clark, H., Commane, R., Daube, B., Diskin, G. W., Elkins, J. W., Gao, R.-S., Gaudel, A., Hintsa, E. J., Johnson, B. J., Kivi, R., McKain, K., Moore, F. L., Parrish, D. D., Querel, R., Ray, E., Sánchez, R., Sweeney, C., Tarasick, D. W., Thompson, A. M., Thouret, V., Witte, J. C., Wofsy, S. C., and Ryerson, T. B.: Global-scale distribution of ozone in the remote troposphere from the ATom and HIPPO airborne field missions, Atmos. Chem. Phys., 20, 10611–10635, https://doi.org/10.5194/acp-20-10611-2020, 2020.

Buonaccorsi, J. P.: Measurement error: models, methods, and applications. CRC press. Cochran, W. G. (1968). Errors of measurement in statistics. Technometrics, 10(4), 637-666, 2010.

Cazorla, M.: Ozone structure over the equatorial Andes from balloon-borne observations and zonal connection with two tropical sea level sites, J Atmos Chem, 74, https://doi.org/10.1007/s10874-016-9348-2, 2017.

Cazorla, M., Parra, R., Herrera, E., and da Silva, F. R.: Characterizing ozone throughout the atmospheric column over the tropical Andes from in situ and remote sensing observations, Elementa, 9, https://doi.org/10.1525/elementa.2021.00019, 2021a.

Chandra S, Ziemke, JR and Min, W et al.: Effects of 1997–1998 El Niño on tropospheric ozone and water vapor. Geophys Res Lett, 25:3867–70, 1998.

1157 Chang, K. L., Cooper, O. R., Gaudel, A., Petropavlovskikh, I., & Thouret, V.: Statistical
1158   regularization for trend detection: an integrated approach for detecting long-term trends from
1159   sparse tropospheric ozone profiles. Atmospheric Chemistry and Physics, 20(16), 9915-9938,
1160   2020

1162 Chang, K. L., Schultz, M. G., Lan, X., McClure-Begley, A., Petropavlovskikh, I., Xu, X., &
1163   Ziemke, J. R.: Trend detection of atmospheric time series: Incorporating appropriate
1164   uncertainty estimates and handling extreme events. Elem Sci Anth, 9(1), 00035, 2021.

1166 Chang, K. L., Cooper, O. R., Gaudel, A., Allaart, M., Ancellet, G., Clark, H., ... & Torres, C.:
1167   Impact of the COVID-19 Economic Downturn on Tropospheric Ozone Trends: An
1168   Uncertainty Weighted Data Synthesis for Quantifying Regional Anomalies Above Western
1169   North America and Europe. AGU Advances, 3(2), e2021AV000542, 2022.

1171 Chang, K.-L., M. G. Schultz, G. Koren and N. Selke: Guidance note on best statistical practices
1172   for TOAR analyses. Available at: https://igacproject.org/activities/TOAR/TOAR-II, 2023.

1174 Cooper, O. R., J. R. Ziemke, and K.-L. Chang: Tropospheric Ozone [in "State of the Climate in
1175   2021"]. Bull. Amer. Meteor. Soc. 103 (8), S96–S98, https://doi.org/10.1175/BAMS-D-22-
1176   0092.1, 2022.

1178 Craigmile, P. F., & Guttorp, P.: A combined estimate of global temperature. Environmetrics,
1179   e2706, 2021.

1181 Cuesta, J., Eremenko, M., Liu, X., Dufour, G., Cai, Z., Höpfner, M., von Clarmann, T., Sellitto,
1182   P., Forêt, G., Gaubert, B. and Beekmann, M.: Satellite observation of lowermost tropospheric
1183   ozone by multispectral synergism of IASI thermal infrared and GOME-2 ultraviolet
1184   measurements over Europe. Atmospheric Chemistry and Physics, 13(19), pp.9675-9693,
1185   2013.

1187 Davis, S.M., Hegglin, M.I., Fujiwara, M., Dragani, R., Harada, Y., Kobayashi, C., Long, C.,
1188   Manney, G.L., Nash, E.R., Potter, G.L. and Tegtmeier, S.: Assessment of upper
1189   tropospheric and stratospheric water vapor and ozone in reanalyses as part of S-
1190   RIP. Atmospheric Chemistry and Physics, 17(20), pp.12743-12778, 2017.

1192 Darras S., Granier C., Liousse C., Boulanger D., Elguindi N., et al.. 2018. The ECCAD database,
1193   version 2: Emissions of Atmospheric Compounds & Compilation of Ancillary Data.

1195 DeMazière, M., Thompson A. M., Kurylo, M. J., Wild, J., Bernhard, G., Blumenstock, T.,
1196   Hannigan, J., Lambert, J-C., Leblanc, T., McGee, T., Nedoluha, G., Petropavlovskikh, I.,
1197   Seckmeyer, G., Simon, P. C., Steinbrecht, W., Strahan, S., and Sullivan, J. T.: The
1198   Network for the Detection of Atmospheric Composition Change (NDACC): History,
1199   status and perspectives, Atmos. Chem. Phys., acp-2017-402, 2018.

1200

1201 Doherty RM, Stevenson DS, Johnson CE, Collins WJ, Sanderson MG: Tropospheric ozone and
1202   El Niño–Southern Oscillation: Influence of atmospheric dynamics, biomass burning
1203   emissions, and future climate change. J. Geophys. Res **111**: D19304.
1204   doi:10.1029/2005JD006849, 2006.

1205

1206 Doniki, S., Hurtmans, D., Clarisse, L., Clerbaux, C., Worden, H. M., Bowman, K. W., and
1207   Coheur, P.-F.: Instantaneous longwave radiative impact of ozone: an application on
1208   IASI/MetOp observations, Atmos. Chem. Phys., 15, 12971–12987,
1209   https://doi.org/10.5194/acp-15-12971-2015, 2015.

1210

1211 Elshorbany, Y. Y, H. C. Kapper, J. R. Ziemke, S. A. Parr, The Status of Air Quality in the
1212   United States during the COVID-19 Pandemic: A Remote Sensing Perspective, Rem.
1213   Sens., 13(3), 369, https://doi.org/10.3390/rs13030369, 2021.

1214

1215 Feng, X., He, X., & Hu, J.: Wild bootstrap for quantile regression. Biometrika, 98(4), 995-999,
1216   2011.

1217

1218 Fleming, Z. L., R. M. Doherty, E. von Schneidemesser, C. S. Malley, et al.: Tropospheric Ozone
1219   Assessment Report: Present-day ozone distribution and trends relevant to human health,
1220   Elem Sci Anth, 6(1):12, DOI: https://doi.org/10.1525/elementa.273, 2018.

1221

1222 Fiore, A.M., Jacob, D.J., Field, B.D., Streets, D.G., Fernandes, S.D. and Jang, C.: Linking ozone
1223   pollution and climate change: The case for controlling methane. Geophysical Research
1224   Letters, 29(19), pp.25-1, 2002.

1225

1226 Fiore, Arlene M., Sarah E. Hancock, Jean-François Lamarque, Gustavo P. Correa, Kai-Lan
1227   Chang, Muye Ru, Owen R. Cooper, Audrey Gaudel, Lorenzo M. Polvani, Bastien
1228   Sauvage and Jerry R. Ziemke: Understanding recent tropospheric ozone trends in the
1229   context of large internal variability: A new perspective from chemistry-climate model
1230   ensembles, Environmental Research: Climate, https://doi.org/10.1088/2752-5295/ac9cc2,
1231   2022.

1232

1233 Fischer, E.V., Jaffe, D.A. and Weatherhead, E.C.: Free tropospheric peroxyacetyl nitrate (PAN)
1234   and ozone at Mount Bachelor: potential causes of variability and timescale for trend
1235   detection. Atmospheric Chemistry and Physics, 11(12), pp.5641-5654, 2011.

1236

1237 Fishman, J., Minnis, P., and Reichle, H. G.: Use of satellite data to study tropospheric ozone in
1238   the tropics, J. Geophys. Res., 91(D13), 14451– 14465, doi:10.1029/JD091iD13p14451,
1239   1986.

1240

Fishman, J., and Larsen, J. C.: Distribution of total ozone and stratospheric ozone in the tropics: Implications for the distribution of tropospheric ozone, J. Geophys. Res., 92(D6), 6627– 6634, doi:10.1029/JD092iD06p06627, 1987.

Fishman, J., Watson, C. E., Larsen, J. C., and Logan, J. A.: Distribution of tropospheric ozone determined from satellite data, J. Geophys. Res., 95(D4), 3599– 3617, doi:10.1029/JD095iD04p03599, 1990.

Fishman, J., Brackett, V.G. and Fakhruzzaman, K.: Distribution of tropospheric ozone in the tropics from satellite and ozonesonde measurements. Journal of atmospheric and terrestrial physics, 54(5), pp.589-597, 1992.

Fishman, J., V. G. Brackett, E. V. Browell and W. B. Grant: Tropospheric ozone derived from TOMS/SBUV measurements during TRACE A, J. Geophys. Res., 101(D19), or https://agupubs.onlinelibrary.wiley.com/doi/abs/10.1029/95JD03576, 1996.

Gaudel, A., O. R. Cooper, et al.: Tropospheric Ozone Assessment Report: Present-day distribution and trends of tropospheric ozone relevant to climate and global atmospheric chemistry model evaluation, Elem. Sci. Anth., 6(1):39, DOI: https://doi.org/10.1525/elementa.291, 2018.

Gaudel, A., Cooper, O.R., Chang, K.L., Bourgeois, I., Ziemke, J.R., Strode, S.A., Oman, L.D., Sellitto, P., Nédélec, P., Blot, R. and Thouret, V.: Aircraft observations since the 1990s reveal increases of tropospheric ozone at multiple locations across the Northern Hemisphere. Science Advances, 6(34), p.eaba8272, 2020.

Gomes, D. G. (2022). Should I use fixed effects or random effects when I have fewer than five levels of a grouping factor in a mixed-effects model?. PeerJ, 10, e12794.

Griffiths, P.T. et al.: Tropospheric ozone in CMIP6 Simulations. Atmospheric Chemistry and Physics, 21(5), 4187–4218, doi:10.5194/acp21-4187-2021, 2021.

Grubbs, F. E.: Errors of measurement, precision, accuracy and the statistical comparison of measuring instruments. Technometrics, 15(1), 53-66, 1973.

Gulev, S.K., P.W. Thorne, J. Ahn, F.J. Dentener, C.M. Domingues, S. Gerland, D. Gong, D.S. Kaufman, H.C. Nnamchi, J. Quaas, J.A. Rivera, S. Sathyendranath, S.L. Smith, B. Trewin, K. von Schuckmann, and R.S. Vose: Changing State of the Climate System. In Climate Change 2021: The Physical Science Basis. Contribution of Working Group I to the Sixth Assessment Report of the Intergovernmental Panel on Climate Change [Masson-Delmotte, V., P. Zhai, A. Pirani, S.L. Connors, C. Péan, S. Berger, N. Caud, Y. Chen, L. Goldfarb, M.I. Gomis, M. Huang, K. Leitzell, E. Lonnoy, J.B.R. Matthews, T.K. Maycock, T. Waterfield, O. Yelekçi, R. Yu, and B. Zhou (eds.)]. Cambridge

University Press, Cambridge, United Kingdom and New York, NY, USA, pp. 287–422, doi:10.1017/9781009157896.004, 2021.

Heue, K-P, et al.: Trends of tropical tropospheric ozone from 20 years of European satellite measurements and perspectives for the Sentinel-5 Precursor. Atmos. Meas. Tech. 9: 5037–5051. DOI: https://doi. org/10.5194/amt-9-5037-2016, 2016.

Hogan, K.B., Hoffman, J.S. and Thompson, A.M.: Methane on the greenhouse agenda. Nature, 354, pp.181-182, 1991.

Hubert, D., Heue, K.P., Lambert, J.C., Verhoelst, T., Allaart, M., Compernolle, S., Cullis, P.D., Dehn, A., Félix, C., Johnson, B.J. and Keppens, A.: TROPOMI tropospheric ozone column data: geophysical assessment and comparison to ozonesondes, GOME-2B and OMI. Atmospheric Measurement Techniques, 14(12), pp.7405-7433, 2021.

Hughes, I., & Hase, T.: Measurements and their uncertainties: a practical guide to modern error analysis. OUP Oxford, 2010.

Jenkins, GS, Gueye, M, Drame, MS & Ndiaye, SA 2014: Evidence of a LNO_X influence on middle/upper troposphere ozone-mixing ratios at Dakar, senegal during Northern Hemisphere summer season, Atmospheric Science Letters, vol. 15, no. 3, pp. 195-203. https://doi.org/10.1002/asl2.489, 2014.

Kley, D., Crutzen, P.J., Smit, H.G.J., Vömel, H., Oltmans, S.J., Grassl, H. and Ramanathan, V.: Observations of near-zero ozone concentrations over the convective Pacific: Effects on air chemistry. Science, 274(5285), pp.230-233, 1996.

Koenker, R., & Hallock, K. F.: Quantile regression. Journal of Economic Perspectives, 15(4), 143-156, 2001.

Krishnamurti, T.N., Sinha, M.C., Kanamitsu, M., Oosterhof, D., Fuelberg, H., Chatfield, R., Jacob, D.J. and Logan, J.: Passive tracer transport relevant to the TRACE A experiment. Journal of Geophysical Research: Atmospheres, 101(D19), pp.23889-23907, 1996.

Lannuque, V., Sauvage, B., Barret, B., Clark, H., Athier, G., Boulanger, D., Cammas, J.P., Cousin, J.M., Fontaine, A., Le Flochmoën, E. and Nédélec, P.: Origins and characterization of CO and O 3 in the African upper troposphere. Atmospheric chemistry and physics, 21(19), pp.14535-14555, 2021.

Leventidou, E., Weber, M., Eichmann, K.-U., Burrows, J. P., Heue, K.-P., Thompson, A. M., and Johnson, B. J.: Harmonisation and trends of 20-year tropical tropospheric ozone data, Atmos. Chem. Phys., 18, 9189-9205, https://doi.org/10.5194/acp-18-9189-2018, 2018.

1325 Liu, J., Strode, S. A., Liang, Q., Oman, L. D., Colarco, P. R., Fleming, E. L., et al.: Change in
1326   tropospheric ozone in the recent decades and its contribution to global total ozone, Journal of
1327   Geophysical Research: Atmospheres, 127, e2022JD037170.
1328   https://doi.org/10.1029/2022JD037170, 2022.

1329

1330 Logan, J. A.: An analysis of ozonesonde data for the troposphere: Recommendations for testing
1331   3-D models and development of a gridded climatology for tropospheric ozone, J. Geophys.
1332   Res.-Atmos., 104, 16115–16149, 1999.

1333

1334 Mastrandrea, M. D., Field, C. B., Stocker, T. F., et al.: Guidance note for lead authors of the
1335   IPCC Fifth Assessment Report on consistent treatment of uncertainties. Intergovernmental
1336   Panel on Climate Change. Available at
1337   https://www.ipcc.ch/site/assets/uploads/2017/08/AR5_Uncertainty_Guidance_Note.pdf,
1338   2010

1339

1340 Mead, M.I., Castruccio, S., Latif, M.T., Nadzir, M.S.M., Dominick, D., Thota, A. and Crippa, P.:
1341   Impact of the 2015 wildfires on Malaysian air quality and exposure: a comparative study of
1342   observed and modeled data. Environmental Research Letters, 13(4), p.044023, 2018.

1343

1344 Mills, G., H. Pleijel, C. S. Malley, B. Sinha, et al.: Tropospheric Ozone Assessment Report:
1345   Present-day tropospheric ozone distribution and trends relevant to vegetation, Elem. Sci.
1346   Anth., 6(1):47, DOI: https://doi.org/10.1525/elementa.302, 2018.

1347

1348 Miyazaki, K., Bowman, K., Sekiya, T., Eskes, H., Boersma, F., Worden, H., Livesey, N., Payne,
1349   V.H., Sudo, K., Kanaya, Y. and Takigawa, M.: Updated tropospheric chemistry reanalysis
1350   and emission estimates, TCR-2, for 2005–2018. Earth System Science Data, 12(3), pp.2223-
1351   2259, 2020.

1352

1353 Moffat, R. J.: Describing the uncertainties in experimental results. Experimental thermal and
1354   fluid science, 1(1), 3-17, 1988.

1355

1356 N. R. Nalli et al., "Validation of Atmospheric Profile Retrievals from the SNPP NOAA-Unique
1357   Combined Atmospheric Processing System. Part 2: Ozone," in IEEE Transactions on
1358   Geoscience and Remote Sensing, vol. 56, no. 1, pp. 598-607, Jan. 2018, doi:
1359   10.1109/TGRS.2017.2762600, 2018.

1360

1361 Nédélec, P., Blot, R., Boulanger, D., Athier, G., Cousin, J.M., Gautron, B., Petzold, A., Volz-
1362   Thomas, A. and Thouret, V.: Instrumentation on commercial aircraft for monitoring the
1363   atmospheric composition on a global scale: the IAGOS system, technical overview of
1364   ozone and carbon monoxide measurements. Tellus B: Chemical and Physical
1365   Meteorology, 67(1), p.27791, 2015.

1366

Nguyen, H. et al.: Spatio-temporal data fusion for very large remote sensing datasets, Technometrics, 56.2 (2014): 174-185, 2014.

Ogino, S.-Y., Miyazaki, K., Fujiwara, M., Nodzu, M. I., Shiotani, M., Hasebe, F., et al.: Cause of a lower-tropospheric high-ozone layer in spring over Hanoi. Journal of Geophysical Research: Atmospheres, 127, e2021JD035727. https://doi-org.colorado.idm.oclc.org/10.1029/2021JD035727, 2022.

Oman, L. D., Douglass, A. R., Ziemke, J. R., Rodriguez, J. M., Waugh, D. W., and Nielsen, J. E.: The ozone response to ENSO in Aura satellite measurements and a chemistry-climate simulation, J. Geophys. Res., 118, 965– 976, doi:10.1029/2012JD018546, 2013.

Oltmans, S.J., Johnson, B.J., Harris, J.M., Vömel, H., Thompson, A.M., Koshy, K., Simon, P., Bendura, R.J., Logan, J.A., Hasebe, F. and Shiotani, M.: Ozone in the Pacific tropical troposphere from ozonesonde observations. Journal of Geophysical Research: Atmospheres, 106(D23), pp.32503-32525. https://agupubs.onlinelibrary.wiley.com/doi/pdfdirect/10.1029/2000JD900834, 2001.

Paton-Walsh Clare, Kathryn M. Emmerson, Rebecca M. Garland, Melita Keywood, Judith J. Hoelzemann, Nicolás Huneeus, Rebecca R. Buchholz, Ruhi S. Humphries, Katye Altieri, Julia Schmale, Stephen R. Wilson, Casper Labuschagne, Egide Kalisa, Jenny A. Fisher, Nicholas M. Deutscher, Pieter G. van Zyl, Johan P. Beukes, Warren Joubert, Lynwil Martin, Thumeka Mkololo, Cybelli Barbosa, Maria de Fatima Andrade, Robyn Schofield, Marc D. Mallet, Mike J. Harvey, Paola Formenti, Stuart J. Piketh, Gustavo Olivares: Key challenges for tropospheric chemistry in the Southern Hemisphere. Elementa: Science of the Anthropocene 4 January 2022; 10 (1): 00050. doi: https://doi.org/10.1525/elementa.2021.00050, 2022.

Pope R., et al.: Investigation of spatial and temporal variability in lower tropospheric ozone from RAL Space UV-Vis satellite products, ACP, in-press; submitted version: https://doi.org/10.5194/egusphere-2023-1172, 2023.

Rabinovich, S. G.: Measurement errors and uncertainties: theory and practice. Springer Science & Business Media, 2006.

Sanhueza, E., Fernández, E., Donoso, L. and Romero, J., 2000. Boundary layer ozone in the tropical America northern hemisphere region. *Journal of atmospheric chemistry*, *35*, pp.249-272.

Saunois, M., Emmons, L., Lamarque, J.-F., Tilmes, S., Wespes, C., Thouret, V., and Schultz, M.: Impact of sampling frequency in the analysis of tropospheric ozone observations, Atmos. Chem. Phys., 12, 6757–6773, 2012.

1408 Sauvage, B., Thouret, V., Cammas, J.P., Gheusi, F., Athier, G. and Nédélec, P.: Tropospheric
1409   ozone over Equatorial Africa: regional aspects from the MOZAIC data. Atmospheric
1410   Chemistry and Physics, 5(2), pp.311-335, 2005.
1411
1412 Sauvage, B., Martin, R. V., van Donkelaar, A., Liu, X., Chance, K., Jaeglé, L., Palmer, P. I., Wu,
1413   S., and Fu, T.-M. (2007a) Remote sensed and in situ constraints on processes affecting
1414   tropical tropospheric ozone, Atmos. Chem. Phys., 7, 815–838,
1415   https://doi.org/10.5194/acp-7-815-2007
1416
1417 Sauvage, B., Martin, R.V., Van Donkelaar, A. and Ziemke, J.R., (2007b) Quantification of the
1418   factors controlling tropical tropospheric ozone and the South Atlantic maximum. Journal
1419   of Geophysical Research: Atmospheres, 112(D11),
1420   **https://doi.org/10.1029/2006JD008008**, 2007.
1421
1422 Seguel, R.J., Castillo, L., Opazo, C., Rojas, N.Y., Nogueira, T., Cazorla, M., Gavidia-Calderón,
1423   M., Gallardo, L., Garreaud, R., Carrasco-Escaff, T. and Elshorbany, Y., 2024. Changes in
1424   South American Surface Ozone Trends: Exploring the Influences of Precursors and
1425   Extreme Events. *EGUsphere*, *2024*, pp.1-25.
1426
1427 Shaddick, G. et al.: Data integration for the assessment of population exposure to ambient air
1428   pollution for global burden of disease assessment, Environmental Science & Technology
1429   52.16 (2018): 9069-9078, 2018.
1430
1431 SHADOZ data, https://doi.org/10.57721/SHADOZ-V06
1432
1433 Singh, R.P. and Chauhan, A., 2020. Impact of lockdown on air quality in India during COVID-
1434   19 pandemic. Air Quality, Atmosphere & Health, 13, pp.921-928.
1435
1436 Skeie, R.B., Myhre, G., Hodnebrog, Ø., Cameron-Smith, P.J., Deushi, M., Hegglin, M.I.,
1437   Horowitz, L.W., Kramer, R.J., Michou, M., Mills, M.J. and Olivié, D.J., 2020: Historical
1438   total ozone radiative forcing derived from CMIP6 simulations. Npj Climate and Atmospheric
1439   Science, 3(1), p.32, 2020.
1440
1441 Smith, N., & Barnet, C. D.: Uncertainty Characterization and Propagation in the Community
1442   Long-Term Infrared Microwave Combined Atmospheric Product System
1443   (CLIMCAPS). Remote Sensing, 11(10), Article 10. https://doi.org/10.3390/rs11101227,
1444   2019.
1445
1446 Smith, N. and Barnet, C. D.: CLIMCAPS observing capability for temperature, moisture, and
1447   trace gases from AIRS/AMSU and CrIS/ATMS, Atmos. Meas. Tech., 13, 4437–4459,
1448   https://doi.org/10.5194/amt-13-4437-2020, 2020.
1449

Sounder SIPS, & Barnet, Chris. (2020a): Sounder SIPS: Suomi NPP CrIMSS Level 2
    CLIMCAPS Full Spectral Resolution: Atmosphere cloud and surface geophysical state
    V2 [Data set]. NASA Goddard Earth Sciences Data and Information Services
    Center. https://doi.org/10.5067/62SPJFQW5Q9B, 2020.

Sounder SIPS, & Barnet, Chris. (2020b). Sounder SIPS: JPSS-1 CrIS Level 2 CLIMCAPS:
    Atmosphere cloud and surface geophysical state V2 [Data set]. NASA Goddard Earth
    Sciences Data and Information Services
    Center. https://doi.org/10.5067/LESQUBLWS18H, 2020.

Stauffer, R. M., A. M. Thompson, J. C. Witte, Characterizing global ozonesonde profile
    variability from surface to the UT/LS with a clustering technique and MERRA-2 reanalysis,
    J. Geophys. Res., 123, doi: 10.1002/2017JD028465, 2018.

Stauffer, R.M., Thompson, A.M., Kollonige, D.E., Witte, J.C., Tarasick, D.W., Davies, J.,
    Vömel, H., Morris, G.A., Van Malderen, R., Johnson, B.J. and Querel, R.R.: A post-2013
    dropoff in total ozone at a third of global ozonesonde stations: Electrochemical
    concentration cell instrument artifacts? Geophysical Research Letters, 47(11),
    p.e2019GL086791, 2020.

Stauffer, R. M., Thompson, A. M., Kollonige, D. E., Tarasick, D. W., Van Malderen, R., Smit,
    H. G. J., et al.: An examination of the recent stability of ozonesonde global network data
    Date Updated: 30 August 2022. Earth and Space Science, 9, e2022EA002459.
    https://doi.org/10.1029/2022EA002459, 2022.

Sterling, C. W., B. J. Johnson, S. J., Oltmans, H. G. J. Smit, A. Jordan, P. D., Cullis, E. G., Hall,
    A. M., Thompson, and J. C. Witte: Homogenizing and Estimating the Uncertainty in
    NOAA's Long Term Vertical Ozone Profile Records Measured with the Electrochemical
    Concentration Cell Ozonesonde, Atmos. Meas. Tech. https://doi.org/10.5194/amt-2017-
    397, 2017.

Szopa, S., V. Naik, B. Adhikary, P. Artaxo, T. Berntsen, W.D. Collins, S. Fuzzi, L. Gallardo, A.
    Kiendler-Scharr, Z. Klimont, H. Liao, N. Unger, and P. Zanis, 2021: Short-Lived Climate
    Forcers. In Climate Change 2021: The Physical Science Basis. Contribution of Working
    Group I to the Sixth Assessment Report of the Intergovernmental Panel on Climate
    Change [Masson-Delmotte, V., P. Zhai, A. Pirani, S.L. Connors, C. Péan, S. Berger, N.
    Caud, Y. Chen, L. Goldfarb, M.I. Gomis, M. Huang, K. Leitzell, E. Lonnoy, J.B.R.
    Matthews, T.K. Maycock, T. Waterfield, O. Yelekçi, R. Yu, and B. Zhou (eds.)].
    Cambridge University Press, Cambridge, United Kingdom and New York, NY, USA, pp.
    817–922, doi:10.1017/9781009157896.008, 2021.

Tarasick, D., Galbally, I.E., Cooper, O.R., Schultz, M.G., Ancellet, G., Leblanc, T., Wallington,
    T.J., Ziemke, J., Liu, X., Steinbacher, M. and Staehelin, J.: Tropospheric Ozone

1493   Assessment Report: Tropospheric ozone from 1877 to 2016, observed levels, trends and
1494   uncertainties. Elementa: Science of the Anthropocene, 7, 2019.
1495

1496 Taylor, J. R., & Thompson, W.: An introduction to error analysis: the study of uncertainties in
1497   physical measurements (Vol. 2, pp. 193-200). Mill Valley, CA: University science books,
1498   1982.

1499 Thompson, A.M. and Cicerone, R.J., 1986a: Atmospheric CH4, CO and OH from 1860 to 1985.
1500   Nature, 321(6066), pp.148-150, 1986.
1501

1502 Thompson, A.M. and Cicerone, R.J., 1986b: Possible perturbations to atmospheric CO, CH4,
1503   and OH. Journal of Geophysical Research: Atmospheres, 91(D10), pp.10853-10864,
1504   1986.
1505

1506 Thompson, A.M., Pickering, K.E., McNamara, D.P., Schoeberl, M.R., Hudson, R.D., Kim, J.H.,
1507   Browell, E.V., Kirchhoff, V.W.J.H. and Nganga, D.: Where did tropospheric ozone over
1508   southern Africa and the tropical Atlantic come from in October 1992? Insights from
1509   TOMS, GTE TRACE A, and SAFARI 1992. Journal of Geophysical Research:
1510   Atmospheres, 101(D19), pp.24251-24278, 1996.
1511

1512 Thompson, A. M., Doddridge, B. G., Witte, J. C., Hudson, R. D., Luke, W. T., Johnson, J. E.,
1513   Johnson, B. J., Oltmans, S. J. and Weller, R.: A tropical Atlantic Paradox: Shipboard and
1514   satellite views of a tropospheric ozone maximum and wave-one in January–February
1515   1999, Geophysical Research Letters, 27(20), 3317–3320, doi:10.1029/1999GL011273,
1516   2000.
1517

1518 Thompson, A.M., Witte, J.C., McPeters, R.D., Oltmans, S.J., Schmidlin, F.J., Logan, J.A.,
1519   Fujiwara, M., Kirchhoff, V.W., Posny, F., Coetzee, G.J. and Hoegger, B.: Southern
1520   hemisphere additional Ozonesondes (SHADOZ) 1998–2000 tropical ozone climatology
1521   1. Comparison with Total ozone mapping spectrometer (TOMS) and ground-based
1522   measurements. Journal of Geophysical Research: Atmospheres, 108(D2), 2003.
1523

1524 Thompson, A. M., and et al.: Southern Hemisphere Additional Ozonesondes (SHADOZ) 1998–
1525   2000 tropical ozone climatology 2. Tropospheric variability and the zonal wave-one, J.
1526   Geophys. Res., 108, 8241, doi:10.1029/2002JD002241, D2, 2003.
1527

1528 Thompson, A. M., et al.: Southern Hemisphere Additional Ozonesondes (SHADOZ) ozone
1529   climatology (2005–2009): Tropospheric and tropical tropopause layer (TTL) profiles
1530   with comparisons to OMI-based ozone products, J. Geophys. Res., 117, D23301,
1531   doi:10.1029/2011JD016911, 2012.
1532

1533 Thompson, A.M., Witte, J.C., Sterling, C., Jordan, A., Johnson, B.J., Oltmans, S.J., Fujiwara,
1534   M., Vömel, H., Allaart, M., Piters, A. and Coetzee, G.J.: First reprocessing of Southern
1535   Hemisphere Additional Ozonesondes (SHADOZ) ozone profiles (1998–2016): 2.

Comparisons with satellites and ground-based instruments. Journal of Geophysical Research: Atmospheres, 122(23), pp.13-000, 2017.

Thompson, A. M., J. C. Witte, C., Sterling, A., Jordan, B. J., Johnson, S. J. Oltmans, ... Thiongo, K.: First reprocessing of Southern Hemisphere Additional Ozonesondes (SHADOZ) ozone profiles (1998-2016): 2. Comparisons with satellites and ground-based instruments. Journal of Geophysical Research: Atmospheres, 122, 13,000-13,025. https://doi.org/10.1002/2017JD027406, 2017.

Thompson, A.M., Stauffer, R.M., Wargan, K., Witte, J.C., Kollonige, D.E. and Ziemke, J.R.: Regional and Seasonal Trends in Tropical Ozone from SHADOZ Profiles: Reference for Models and Satellite Products. Journal of Geophysical Research: Atmospheres, 126(22), p.e2021JD034691, 2021.

Torres, O., Bhartia, P. K., Jethva, H., and Ahn, C.: Impact of the ozone monitoring instrument row anomaly on the long-term record of aerosol products, Atmos. Meas. Tech., 11, 2701–2715, https://doi.org/10.5194/amt-11-2701-2018, 2018.

Tsivlidou, M., Sauvage, B., Barret, B., Wolff, P., Clark, H., Bennouna, Y., Blot, R., Boulanger, D., Nédélec, P., Le Flochmoën, E. and Thouret, V.: Tropical tropospheric ozone and carbon monoxide distributions: characteristics, origins and control factors, as seen by IAGOS and IASI. Atmospheric Chemistry and Physics, pp.1-50, https://doi.org/10.5194/acp-23-14039-2023, 2023.

Veefkind, J., Aben, I., McMullan, K., Förster, H., de Vries, J., Otter, G., Claas, J., Eskes, H., de Haan, J., Kleipool, Q., van Weele, M., Hasekamp, O., Hoogeveen, R., Landgraf, J., Snel, R., Tol, P., Ingmann, P., Voors, R., Kruizinga, B., Vink, R., Visser, H., and Levelt, P.: TROPOMI on the ESA Sentinel-5 Precursor: A GMES mission for global observations of the atmospheric composition for climate, air quality and ozone layer applications, Remote Sens. Environ., 120, 70–83, https://doi.org/10.1016/j.rse.2011.09.027, 2012. a, b, c

Wang, H., Lu, X., Jacob, D. J., Cooper, O. R., Chang, K.-L., Li, K., Gao, M., Liu, Y., Sheng, B., Wu, K., Wu, T., Zhang, J., Sauvage, B., Nédélec, P., Blot, R., and Fan, S.: Global tropospheric ozone trends, attributions, and radiative impacts in 1995–2017: an integrated analysis using aircraft (IAGOS) observations, ozonesonde, and multi-decadal chemical model simulations, Atmos. Chem. Phys., 22, 13753–13782, https://doi.org/10.5194/acp-22-13753-2022, 2022.

Wargan, K., Labow, G., Frith, S., Pawson, S., Livesey, N., and Partyka, G.: Evaluation of the ozone fields in NASA's MERRA-2 reanalysis. Journal of Climate 30, 8, 2961-2988, https://doi.org/10.1175/JCLI-D-16-0699.1, 2017.

Wargan, K., N. Kramarova, B. Weir, S. Pawson, and S. M. Davis: Toward a reanalysis of stratospheric ozone for trend studies: Assimilation of the Aura Microwave Limb Sounder

and Ozone Mapping and Profiler Suite Limb Profiler data, J. Geophys. Res., 125, https://doi.org/10.1029/2019JD031892, 2020.

Weatherhead, E.C., Reinsel, G.C., Tiao, G.C., Meng, X.L., Choi, D., Cheang, W.K., Keller, T., DeLuisi, J., Wuebbles, D.J., Kerr, J.B. and Miller, A.J.: Factors affecting the detection of trends: Statistical considerations and applications to environmental data. Journal of Geophysical Research: Atmospheres, 103(D14), pp.17149-17161, 1998.

Witte, J.C., Thompson, A.M., Smit, H.G., Fujiwara, M., Posny, F., Coetzee, G.J., Northam, E.T., Johnson, B.J., Sterling, C.W., Mohamad, M. and Ogino, S.Y.: First reprocessing of Southern Hemisphere ADditional OZonesondes (SHADOZ) profile records (1998–2015): 1. Methodology and evaluation. Journal of Geophysical Research: Atmospheres, 122(12), pp.6611-6636, 2017.

Witte, J. C., Thompson, A. M., Smit, H. G. J.,Vömel, H., Posny, F., & Stübi, R. :First reprocessing of SouthernHemisphere ADditional OZonesondesprofile records: 3. Uncertainty in ozone profile and total column. Journal ofGeophysical Research: Atmospheres,123,3243–3268, 8. https://doi.org/10.1002/2017JD027791, 2018.

WMO/GAW Report 268, 2021. Ozonesonde Measurement Principles and Best Operational Practices: ASOPOS 2.0 (Assessment of Standard Operating Procedures for Ozonesondes) August 2021, edited by H. G. J. Smit and A. M. Thompson. Available at: https://library.wmo.int/index.php?lvl=notice_display&id=21986#.Y4iiRn3MJc8

Wofsy S.C. et al., ATom: Merged Atmospheric Chemistry, Trace Gases, and Aerosols. ORNL DAAC (2018). https://doi.org/10.3334/ORNLDAAC/1909 (Accessed 1 May,2023).

Wood, S. N. (2017). Generalized additive models: an introduction with R. Chapman and hall/CRC.

Xiong, X., Liu, X., Wu, W., Knowland, K.E., Yang, Q., Welsh, J. and Zhou, D.K.: Satellite observation of stratospheric intrusions and ozone transport using CrIS on SNPP. Atmospheric Environment, p.118956. https://doi.org/10.1016/j.atmosenv.2022.118956, 2022.

Xue, L., A. Ding, O. Cooper, X. Huang, W. Wang, D. Zhou, Z. Wu, A. McClure-Begley, I. Petropavlovskikh, M. O. Andreae, C. Fu: ENSO and Southeast Asian biomass burning modulate subtropical trans-Pacific ozone transport, National Science Review, nwaa132, https://doi.org/10.1093/nsr/nwaa132, 2020.

Yamasoe , M.A., Sauvage B., Thouret V., Nédélec P., Le Flochmoen E., Barret B.: Analysis of tropospheric ozone and carbon monoxide profiles over South America based on MOZAIC/IAGOS database and model simulations, Tellus B: Chemical and Physical Meteorology, 67:1, DOI: 10.3402/tellusb.v67.27884, 2015.

Young, P. J., Archibald, A. T., Bowman, K. W., Lamarque, J.-F., Naik, V., Stevenson, D. S.,
Tilmes, S., Voulgarakis, A., Wild, O., Bergmann, D., Cameron-Smith, P., Cionni, I.,
Collins, W. J., Dalsøren, S. B., Doherty, R. M., Eyring, V., Faluvegi, G., Horowitz, L.
W., Josse, B., Lee, Y. H., MacKenzie, I. A., Nagashima, T., Plummer, D. A., Righi, M.,
Rumbold, S. T., Skeie, R. B., Shindell, D. T., Strode, S. A., Sudo, K., Szopa, S., and
Zeng, G.: Pre-industrial to end 21st century projections of tropospheric ozone from the
Atmospheric Chemistry and Climate Model Intercomparison Project (ACCMIP), Atmos.
Chem. Phys., 13, 2063–2090, https://doi.org/10.5194/acp-13-2063-2013, 2013.

Zhang, Y., Cooper, O.R., Gaudel, A., Thompson, A.M., Nédélec, P., Ogino, S.Y. and West, J.J.:
Tropospheric ozone change from 1980 to 2010 dominated by equatorward redistribution
of emissions, Nature Geoscience, 9(12), pp.875-879, 2016.

Zhang, Y., West, J.J., Emmons, L.K., Flemming, J., Jonson, J.E., Lund, M.T., Sekiya, T., Sudo,
K., Gaudel, A., Chang, K.L. and Nédélec, P.: Contributions of world regions to the global
tropospheric ozone burden change from 1980 to 2010. Geophysical Research
Letters, 48(1), p.e2020GL089184, 2021.

Ziemke, J. R., Chandra, S., and Bhartia, P. K.: Two new methods for deriving tropospheric
column ozone from TOMS measurements: The assimilated UARS MLS/HALOE and
convective-cloud differential techniques, J. Geophys. Res., 103, 22115–22127, 1998.

Ziemke, J. R., Chandra, S., and Bhartia, P. K.: A 25-year data record of atmospheric ozone from
TOMS Cloud Slicing: Implications for trends in stratospheric and tropospheric ozone, J.
Geophys. Res., 110, D15105, doi:10.1029/2004JD005687, 2005.

Ziemke, J.R., Chandra, S., Duncan, B.N., Froidevaux, L., Bhartia, P.K., Levelt, P.F. and Waters,
J.W.: Tropospheric ozone determined from Aura OMI and MLS: Evaluation of
measurements and comparison with the Global Modeling Initiative's Chemical Transport
Model. Journal of Geophysical Research: Atmospheres, 111(D19), 2006.

Ziemke, J. R., Joiner, J., Chandra, S., Bhartia, P. K., Vasilkov, A., Haffner, D. P., Yang, K.,
Schoeberl, M. R., Froidevaux, L., and Levelt, P. F.: Ozone mixing ratios inside tropical
deep convective clouds from OMI satellite measurements, Atmos. Chem. Phys.,
9, 573–583, doi:10.5194/acp-9-573-2009, 2009.

Ziemke, J. R., Chandra, S., Labow, G. J., Bhartia, P. K., Froidevaux, L., and Witte, J. C.: A
global climatology of tropospheric and stratospheric ozone derived from Aura OMI and
MLS measurements, Atmos. Chem. Phys., 11, 9237–9251, doi:10.5194/acp-
11-9237-2011, 2011.

1667   Ziemke, J. R., and Chandra, S.: Development of a climate record of tropospheric and ozone from
1668   satellite remote sensing: Evidence of an early recovery of global stratospheric ozone,
1669   Atmos. Chem. Phys., 12, 5737-5753, doi:10.5194/acp-12-5737-2012, 2012.
1670
1671   Ziemke, J. R., Douglass, A. R., Oman, L. D., Strahan, S. E., and Duncan, B. N.: Tropospheric
1672   ozone variability in the tropics from ENSO to MJO and shorter timescales, Atmos. Chem.
1673   Phys., 15, 8037–8049, https://doi.org/10.5194/acp-15-8037-2015, 2015.
1674
1675   Ziemke, J. R., Oman, L. D., Strode, S. A., et al.: Trends in global tropospheric ozone inferred
1676   from a composite record of TOMS/OMI/MLS/OMPS satellite measurements and the
1677   MERRA-2 GMI simulation , Atmos. Chem. Phys., 19, 3257–3269,
1678   https://doi.org/10.5194/acp-19-3257-2019, 2019.
1679
1680
1681
1682
1683